SYNTHESIS AND FABRICATION OF LASER SCRIBED NANO-COMPOSITES FOR STRAIN SENSING

By

Maham Iqra

School of Chemical and Materials Engineering

National University of Sciences and Technology

July, 2021

SYNTHESIS AND FABRICATION OF LASER SCRIBED NANO-COMPOSITES FOR STRAIN SENSING

Name: Maham Iqra

Reg. No: NUST2017NNSE05-00000204417

This thesis is submitted as a partial fulfillment of the requirements for the degree of

MS in Nanoscience and Engineering

Supervised by: Dr. Mohammad Ali Mohammad

School of Chemical and Materials Engineering (SCME)

National University of Sciences and Technology (NUST)

H-12 Islamabad, Pakistan

July, 2021

DEDICATION

I dedicate my thesis to my family specially my mother Zahida Parveen and my siblings who have been a constant source of support and prayers

ACKNOWLEDGMENTS

“Indeed, in the creation of the heavens and the earth and the alteration of the night and the day are signs for those of understanding” (Quran 3:190)

I would like to thank ALLAH Almighty who is the creator of this world and many others like this. He created this universe for us to explore. With this divine inspiration, I desire to explore as a researcher.

I am really thankful to my supervisor, Dr. Mohammad Ali Mohammad, who inspires me to work hard; his behavior and persistence towards his goals mesmerize me to slog with passion. I am honored to work under his supervision. I am also indebted to my co-supervisor, Dr. Syeda Sitwat Batool, for guiding me throughout my research phases in Characterization to thesis writeup.

I acknowledge my G.E.C members Dr. Sofia Javed and Dr. Aftab Akram for our routine discussions and helping me in characterization and to understand the chemistry behind my research project. I would also like to thank them for providing a stimulating environment for doing my practical work in their lab. I would like to thank my research mates Aamena Qasmi and Sunaina Rafique for useful discussions throughout my research.

I am also thankful to my mother whose strength and hard work always pushes me to do the best and always brace myself to achieve my goals. My siblings Usama Amin and Ayeza Amin also supported me during my thesis, for which I am indebted. I am very thankful for my friends who always motivate me and never let me down. I would like to thank Dr. Raza Ali, and Roshana Naqvi without them I cannot encourage myself to work again. To honor their support, I have invested all my steadfastness to this work.

Maham Iqra

ABSTRACT

Flexible Strain sensors are an important constituent in soft robotics, health care devices and defense industry. In flexible strain sensors, achieving consistency and high sensitivity has always been challenging. A number of materials and their derivatives have been explored to achieve the ultimate balanced sensitivity and strain range.

In this work we have fabricated thin film strain sensor device prepared by drop casting method. A specific intensity laser is used to draw 1 × 1 cm^2 pattern on graphene oxide (GO) to convert it into reduced graphene oxide (RGO). Conversion of GO into RGO causes the material to become conductive and shows piezoresistive behavior upon applying strain. The device is fabricated on polydimethylsiloxane (PDMS) as a base material due to its flexibility and bio compatibility. It can easily stick with the human skin.

A locally made test rig is used to produce the effect of torsion, bending and stretching on the strain sensor device. The resulting resistance change on the device has been measured. The sensitivity is calculated as gauge factor. The gauge factor of torsion, bending and stretching is observed to be 90.3, 3.5 and 12.1 respectively. The corresponding strain ranges are 0-11%, 0-150% and 0-140%. This sensor is found to be providing a balance between strain range and sensitivity. Hand test was performed for the detection of joint muscle movement. Change of resistance has been observed indicating the working performance of the device.

A 2 × 2 pressure sensor array has also been fabricated by availing the same method. Pressure has been detected by manually exerting the pressure on this device. Change of resistance has been calculated by using multi-meter.

These types of strain sensors are used for health monitoring e.g muscle motion of a diseased person, heartbeat and blood pressure measurement.

TABLE OF CONTENTS

Page No.

LIST OF FIGURES

LIST OF TABLES

LIST OF ABBREVIATIONS

	MEANING
AEC	Aluminum Electrolyte Capacitor
BSE	Backscattered Electrons
CNC	Carbon Nano Coils
CNT	Carbon Nanotube
CTE	Coefficient Of Thermal Expansion
CV	Cyclic Voltammetry
CVD	Chemical Vapor Deposition
EBL	Electron Beam Lithography
FTIR	Fourier Transform Infrared Spectroscopy
GO	Graphene Oxide
IBL	Ion Beam Lithography
LSG	Laser Scribed Graphene
MWCNT/MWNT	Multi Wall Carbon Nanotubes
NIL	Nanoimprint Lithography
PAR	Polyarylates
PC	Polycarbonate
PEI	Polyetherimide
PEN	Polyethylene Naphthalate
PEO	Polyethylene Oxide
PES	Polyethersulphone
PET	Polyethylene Terephthalate
PI	Polyimide
PMMA	Polymethyl Methacrylate
PVA	Polyvinyl Alcohol
PVDF	Polyvinylidene Fluoride
OBL	Optical Beam Lithography

RGO	Reduced Graphene Oxide
SBL	Scanning Beam Lithography
HSQ	Hydrogen Silsesquioxane
SEM	Scanning Electron Microscope
SMS	Surface Mountable Supercapacitors
SSG	Self-Stacked-Solvated-Graphene
T_g	Glass Transition Temperature
LCD	Liquid Crystal Displays
PDMS	Polydimethylsiloxane
XRD	X-Ray Diffraction
LiF	Lithium Fluoride
NEMS	Nanoelectromechanical Systems
MEMS	Microelectromechnical Systems
a-Si:H	Hydrogenated Amorphous Silicon
OLED	Organic Light-Emitting Diode
AMLCD	Active-Matrix Liquid-Crystal Display
PSCVD	Plasma Enhanced Chemical Vapor Deposition
ITO	Indium Tin Oxide
E-Skin	Electronic Skin
GF	Gauge Factor
CNS	Carbon Nano Structures
TGFs	Hollow Tubing Graphene Fibers
MCG	Molybdenum-Carbide-Graphene
SBS/FLG	Poly(Styrene-Butadienestyrene)/Fewlayer Graphene
PZT	Lead–Zirconate–Titanate
ECDs	Electrochromic Devices
LEG	Laser-Engraved Graphene
TFT	Thin Film Transistor

CHAPTER 1: INTRODUCTION

Strain sensors were manufactured by Arthur C. Ruge and Edward E. Simmons for the first time in 1938. Since then, they have become one of the most widely used sensor around the world. Estimation of market demand for strain sensors is expected to grow from $193.9 billion in 2020 to $332.8 billion by 2025 with an annual CAGR of 11.4%[1]. Estimation of market value of strain sensors is differentiated by several factors, i.e., the type of strain sensor, the region, and applications of strain sensor. Piezoresistive strain sensors are one of the most sought after technologies these days. China attracts lots of attention in production of piezoresistive type strain sensors[2] by Shanghai Yiling Electrical Measuring Instruments Company. A U.S based company named Vishey InterTechnology, Inc has the highest share of 8.1%, while HBM (Germany) have 7.25% share in the sensor market and Europe based manufacturer Zemic have 5.24% share in the market[3].

Advancement in strain sensor technology along with MEMS fabrication techniques are helping to increase the functionality of strain sensors, while decreasing their size and cost. Furthermore, novel materials are being used, which are enabling further advances in the field. Researchers are printing on flexible materials such as printingon newspapers. These flexible plastics also cost less than conventional materials.

Flexibility factor combined with the good electrical properties can be able to produce electronic devices used for different purposes like defense and aerospace technology[4], artificial throat[5], electronic skin[6], health care issues, heartbeat, blood pressure measurement and eye pressure measurement. It takes a revolutionary part where machines combine with the human containing various properties and flexibility combined with the various sensors to mimic the human skin. This technology has profound implications in prosthetics and has a lot more to merge with. It can also be used on the burned areas of the skin. Flexibility factor influence every field like fabrication of these devices on clothes [7-9], in solar panels etc.

1.1 SENSOR:

In history, we have seen that development in materials and engineering has been driving the sensor industry. Advancement in materials will permit better manipulation in their properties according to the requirement. We can alter their physical and chemical properties to make more accurate and sensitive devices. In the 1860's, Wilhelm von Siemens made a temperature sensor which is considered as the first ever made sensor [10]. In 1883, Warren S. Johnson invented a thermostat that depicts very high sensitivity that has been used to manage the temperature of a specific cabin. Then in the 1940's, infrared sensors had been invented. Motion sensors, invented by Samuel Bagno, are widely used in automatic doors for security purposes from early 1940's till now[11]. This emerging field of sensor technology is expanding in playing an important role in the scientific and technical part of mainly every discipline.

A sensor contains a sensing element which reacts upon any change in the environment resulting in the change of resistance, capacitance, current etc. A transducer then converts and amplifies this change into a readout form that can be visualized on any measuring device. The performance of the sensor depends upon the sensing element, the characteristics of which are described by sensitivity, accuracy, repeatability, response time and operating range, etc. Transducer is then connected to the amplifier in case the signal is too weak to measure. However, sensors are constrained by environmental behavior, packaging and cost, which is a challenge for the researchers.

We are moving towards smarter technology which can be portable, compact and more sensitive. Micro and nano devices made by MEMS and NEMS processing techniques make intricate structures on a single chip resulting in low cost and miniaturized electronics that permits more complex structures to be achieved. To make the device smarter and user friendly, complexities were assembled under a small chip and concealed internally. Smart sensing would set up new opportunities to work on the different modules in a different way or with the variety of materials.

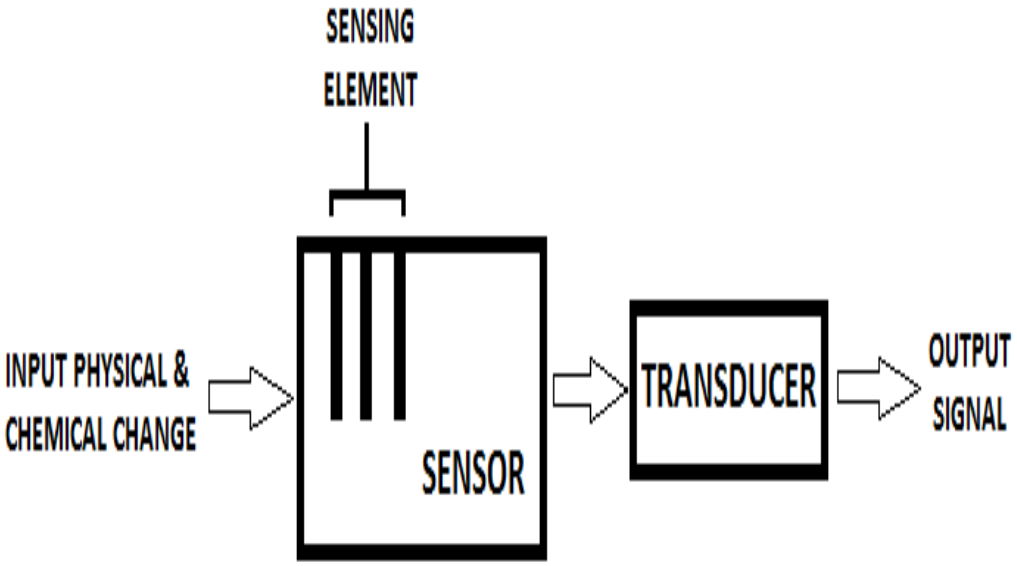

Fig 1: Sensing mechanism for any kind of sensor.

1.1.1 TYPES OF SENSOR:

i. Strain sensor
ii. Pressure sensor
iii. Gas sensor
iv. Temperature sensor
v. Light sensor
vi. Motion sensor

1.2 PRESSURE SENSOR:

In 2017, Asia pacific was the main region to consume a high share in the pressure sensor market. Overall share of sensor technology in 2016 was 7.88 billion dollars which is forecasted to touch 11 billion dollars by 2023. Consumer market has the highest CAGR growth rate of 5.27% [12]. Piezoresistive strain sensors are the highest to grow in this list [13, 14].

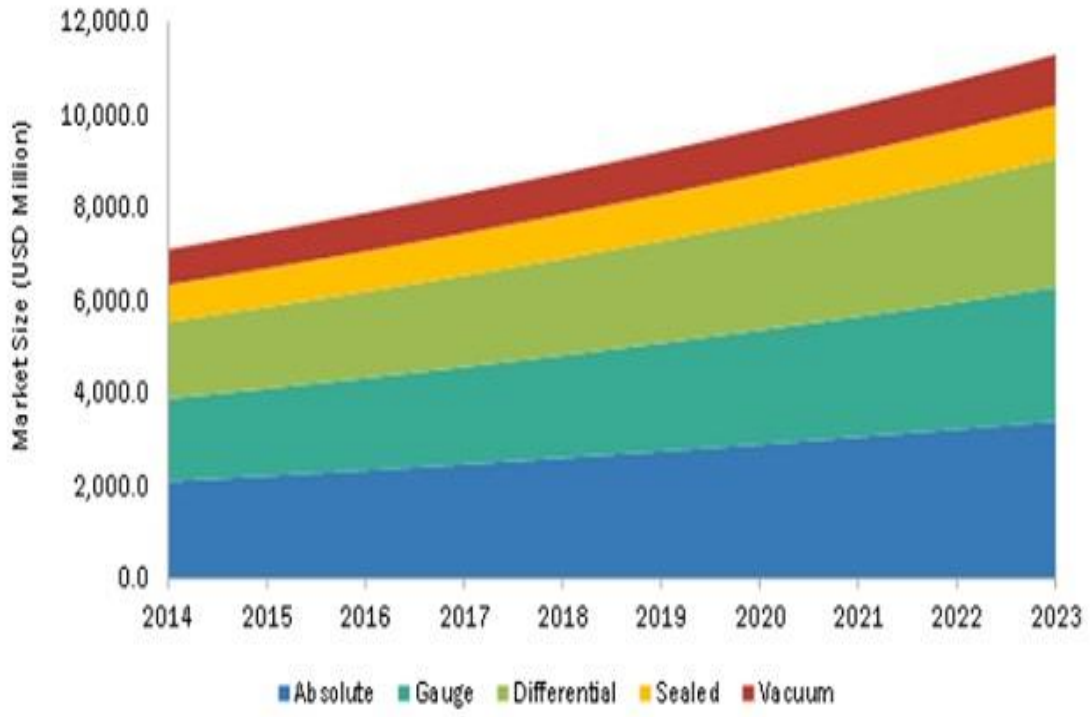

Fig 2: Market value chart from 2014 to 2023[12]

Italian physicist Evangelista Torricelli invented the aneroid barometer in 1643. He was able to measure atmospheric pressure but without knowing the actual reason he concluded it as the force[15, 16].

Pressure sensing technology requires the potential to identify the magnitude of the applied force. The first technology of pressure sensor was mechanically formed and contains bourdon tube gauges that deflect a needle according to the magnitude of the pressure. The deflection of diaphragm increases by increasing pressure. This is a kind of elementary/basic pressure sensor in modern pressure sensors, output is measured electrically using strain gauge and pressure transducers [17]. That can also be measured digitally or by analogue method which requires a proper circuiting system.

Smart emerging technology requires advancement in these three parts of the pressure sensor; **sensor** & **transducer element, packaging material** and **electronics device** which imitate the skin's novel facets including flexibility, durability and sensitivity. This work is specifically on the sensitivity of sensor elements as the properties of the material require work on this aspect of the sensor.

In case of pressure sensor sensitivity measures in the form of differential pressure, On the basis of which it is further categorized into three types of pressure sensing element [16, 18].

i. Absolute

The applied pressure is measured with respect to zero (absolute vacuum). Sensors contain only one path for entering the media to exert pressure on the sensing element. [8] which leads to the positive change in output that is directly related to the applied pressure. It is used for the measurement of pressure that will operate at different altitudes because it measures more precisely than a gauge pressure sensor. The atmosphere applied 760mmHg absolute pressure on the sea level [16].

ii. Differential

It measures the pressure difference similar to gauge but the difference here is that the reference point is inside the system other that absolute and atmosphere. Pressure difference proportionally causes the output to be positive and negative. It is usually used to measure the pressure difference between two points or objects.

iii. Gauge

It quantifies the pressure relative to ambient pressure mainly at atmospheric conditions. It can be positive for pressures higher than atmospheric, or negative for lower pressures. It gives the positive value for pressure higher than atmospheric pressure and negative for the rest. Strain gauge provides precision from 0.03% to 0.25% full scale and is opted for almost all industrial and defense applications [19]. The reason of selecting this method is that we do not require specific vacuum conditions which not also increase the cost but is also hard to maintain in most of the devices.

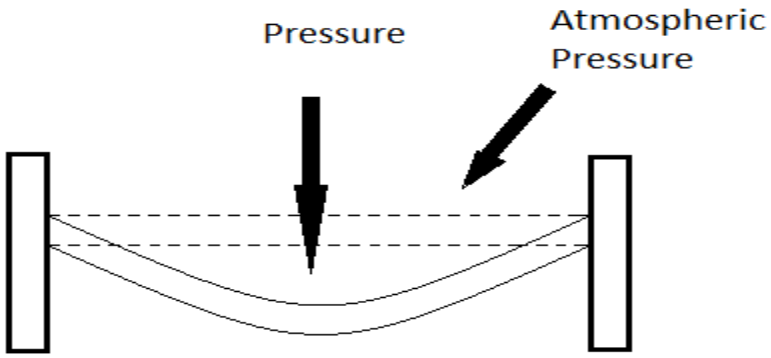

Fig 3: Illustration of impact of pressure on pressure gauge

We are capable of making smaller devices by using MEMS fabrication technique. In the case of a pressure sensor the basic element is a deformable diaphragm containing piezoresistive material formed into a piezoresistor by ion implantation or ion-diffusion method [20]. Pressure range depends upon the diaphragm material which bears the pressure in the range of their deformability. Upon applying pressure to the sensor, resistivity changes which alters the conductivity and that can be measured with output measuring device.

1.3 STRAIN SENSOR:

The strain sensor was first invented in 1938 by Edward E., Simmons and Authur C. Ruge [21]. Strain depicts the change in length or angle under applied stress. This includes compression, bending, torsion etc. as shown in Fig 4.

The device consists of an electrically active material that is fabricated on the substrate of choice, thus used to sense the strain by electrical, resistance, capacitance or inductance change. The most common strain sensor is the piezoresistive strain sensor. These sensors detect the strain by detecting the change in resistance caused by the strain. A precise amount of input in the form of electrical source is provided to the strain to measure change in resistance. This resistance is then measured as an output.

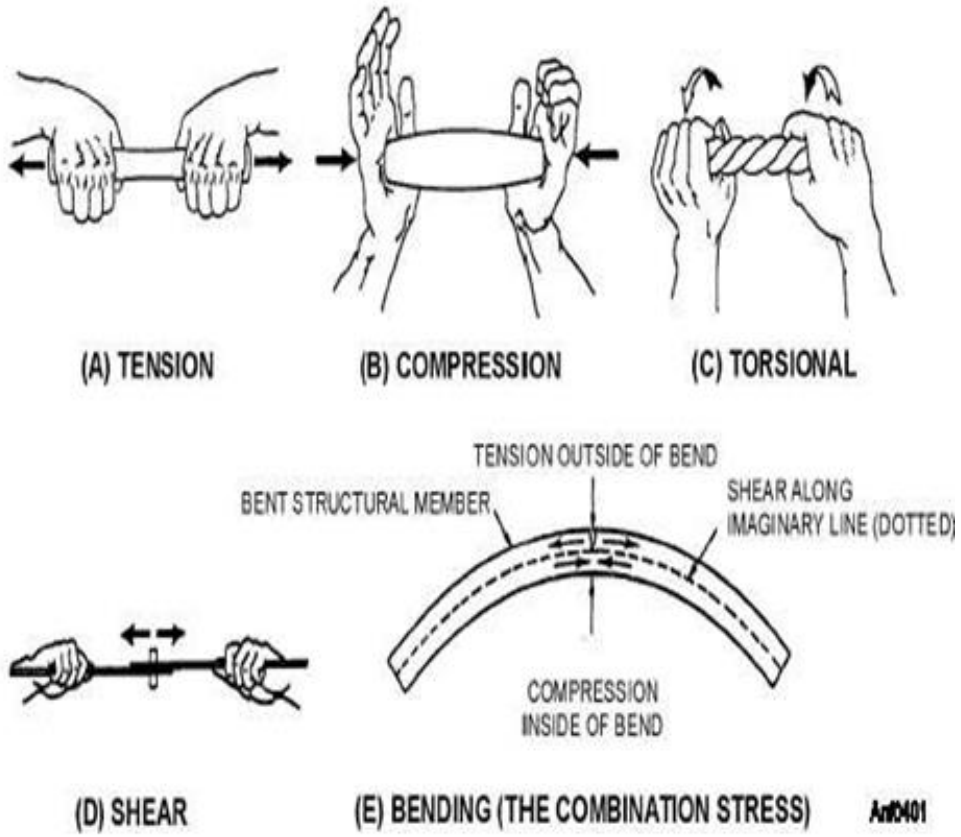

Fig 4: Types of different strain [22]

1.3.1 STRAIN SENSTIVITY:

Strain can be monitored in the form of resistance, capacitance and electrical change as a consequence of applying any kind of pressure such as stretching, compression, torsion and bending. The sensitivity of these devices can be appraised by gauge factor (GF). GF can be represented by

$$G.F = \frac{(\Delta R)}{R^i \varepsilon} \text{\_\_\_\_\_(i)}$$

ΔR is the change in resistance from final resistance of the device to initial and can be expressed as $\Delta R = R^f - R^i$, where R^i represents the initial resistance when no stress is applied to the device and R^f is the final resistance after objected to stress. While the quantity ε is the strain applied on the device by means of length change in stretching, compression and bending and as an angle when we apply torsion stress and can be expressed as $\varepsilon = \Delta L / L^i$. Here $\Delta L = L^f - L^i$ where L^f is the final length and L^i is the initial length.

1.3 BACKGROUND OF ELECTRONIC SKIN:

The initial research on electronic skin started in the 1970s when the first touch sensitive prosthetic arm was made. Fiction inspired us to make touch screen computers in the early 1980's and till now lots of work has been done on this area but still some factors need to be addressed and also some modifications are required in making flexible electronic skin.

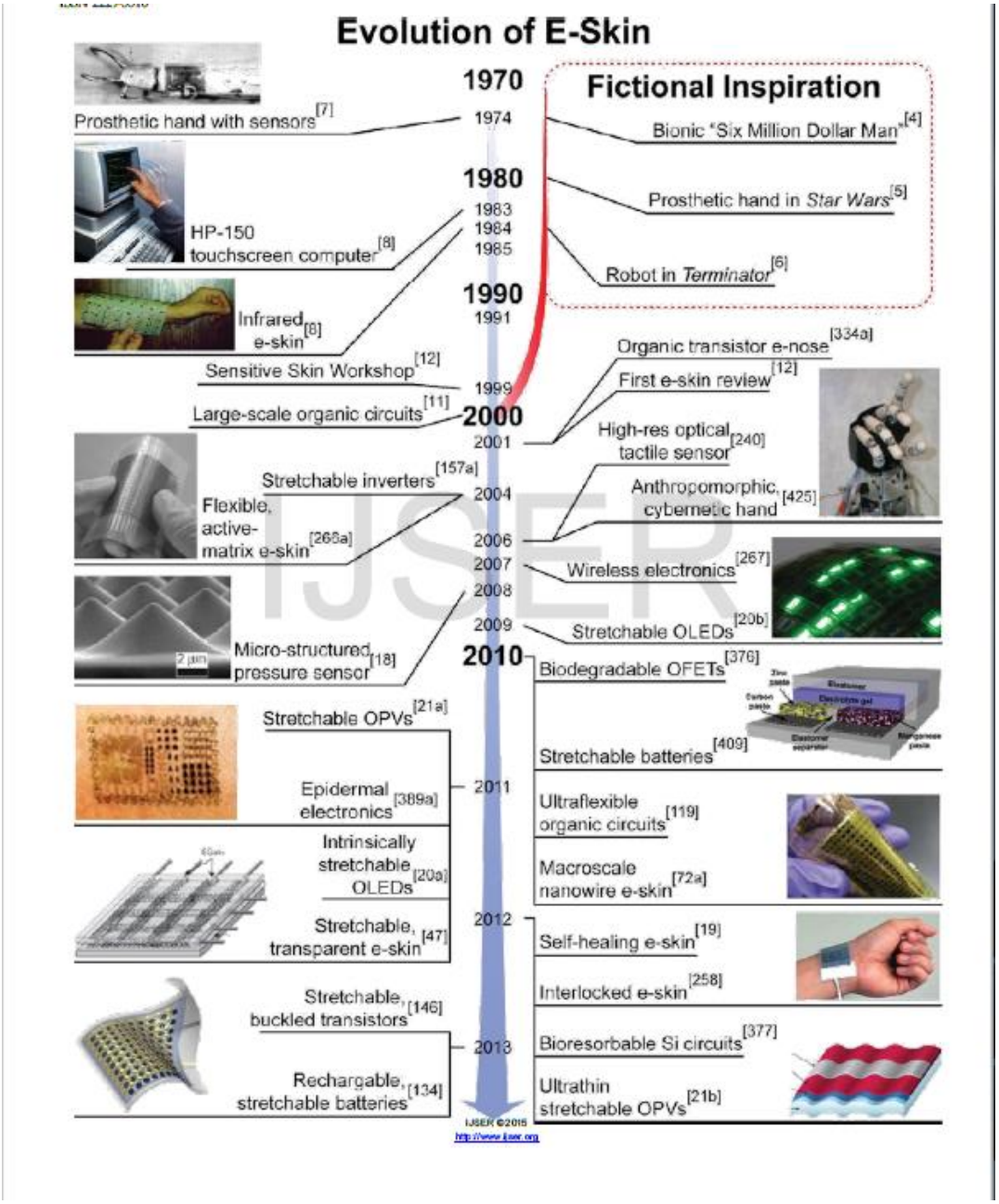

Fig 5: Evolution of electronic skin for last 65 years [23]

1.4.1 ARTIFICIAL ELECTRONIC SKIN:

Human skin is a very important and complex organ which contains flexibility factors including with many other sensors. Bio-inspired electronic skin was explored in science fiction few years back but now advancement has come to a level where actual devices are available in the market these days. At this time prosthetics lack the ability to sense the touching area so there is a need for electronic skin technology that mimics the shape of the object on the surface of the tactile sensor. Usually a set of sensor elements are put together in an array to form a skin like structure. These sensors are combined together by copper wires to make connections for the measurement of the pressure. These array structures play the role in mimicking the object rather than the single pressure sensor. This is the fundamental process of future generation of electronic skin. Many investigators are trying to make the device with higher credibility, faster response by trying different ways of putting various combinations of elements arranged to make array structures that could lead to various applications like prosthetics, health monitoring, robotics and many more. There are numerous diseases which require real time monitoring that directly relates to human life. Skin like properties allocate real time surveillance and round the clock monitoring of diseases by embedding on t-shirts or in a bracelet.

Fig 6: Electronic skin mounted on artificial hand [24]

1.5 FLEXIBLE ELECTRONICS:

Flexible electronics technology has recently been introduced in the market. They have the advantage over normal electronics due to their low-cost fabrication. Flexible electronics reduces the burden on circuits by fabricating the device on plastics, woven fabric, etc. It's the assembling of electronic components on flexible substrates. It is an emerging technology that is expected to enable the growth of a new industry. So why are people so excited about flexible electronics? The key factor is ubiquitously low manufacturing cost and the compact portable structure that may enable product innovation in case one is printing on the flexible substrate and get this flexible form factor and this gives you some significance latitude of product innovation. To manufacture these types of electronics we usually use printing technology. The advantage of using this technology is we can design any kind of structure and then if it doesn't go well, we can reprint another design that leads to a source of rapid prototyping.

Materials that are used to make the device needs to be functionalized differently to take into account both mechanical and electrical attributes. Functionality causes variation in the use of the material e.g. it can also be used to match the young's modulus of both electrical and substrate material for better adhesion. We can also scribe GO by laser to convert the GO into electrically active material.

1.5.1 BACKGROUND OF FLEXIBLE ELECTRONICS:

Leather is the first flexible material used for writing purpose before the paper has been made. First flexible solar cell was made by thinning the silicon wafer to ∼100 μm and put together on a flexible substrate. The 1973 energy crisis motivated scientists to reduce the cost of photovoltaic electricity [25]. The early 1980s period was the time when flexibility was introduced in n+–i a-Si:H/Pt Schottky barrier and p+–i–n+ a-Si:H/ITO solar cells by Plattner et al. [26] and by Okaniwa et al. [27-29].

A Japan based firm worked on the active-matrix liquid-crystal display (AMLCD) in the mid 1980's by utilizing the large-area plasma enhanced chemical vapor deposition (PECVD) machines that has been formulated for the reduction of a-Si:H solar cells. For the first time in 1994, Constant et al. at Iowa State University manifested a-Si:H

TFT(thin film transistor) on PI substrate [30]. From then researchers and companies are working on the formation of the working flexible devices. For example, in 2005 Philips took a first step to commercialize their product in the market ‘a rollable electrophoretic display’ and Samsung presented a 7 inches prototype flexible liquid crystal panel [31]. In 2006, Palo Alto Research Center and the Universal Display Corporation introduced a paradigm flexible organic light-emitting diode (OLED) a poly-Si TFT backplane display which shows full-color and full-motion mounted on steel foil [32, 33].

1.5.2 APPLICATION OF FLEXIBLE ELECTRONICS:

Flexible electronics have diverse application fields such as the use of wearable medical equipment for health monitoring. Such equipment is potable and generates a quick response upon any serious condition before it’s been too late to rush to the hospital. Flexible solar cells are also fabricated these days, which are more efficient and moldable to be used as shades on buildings. Flexible electronic flat panel displays are seeking attention these days. Companies like Samsung and Royole launched the first foldable phones in the market. Flexible electronics are used with fabrics to merge the devices with clothes for health care purpose mainly referred to as E-textiles.

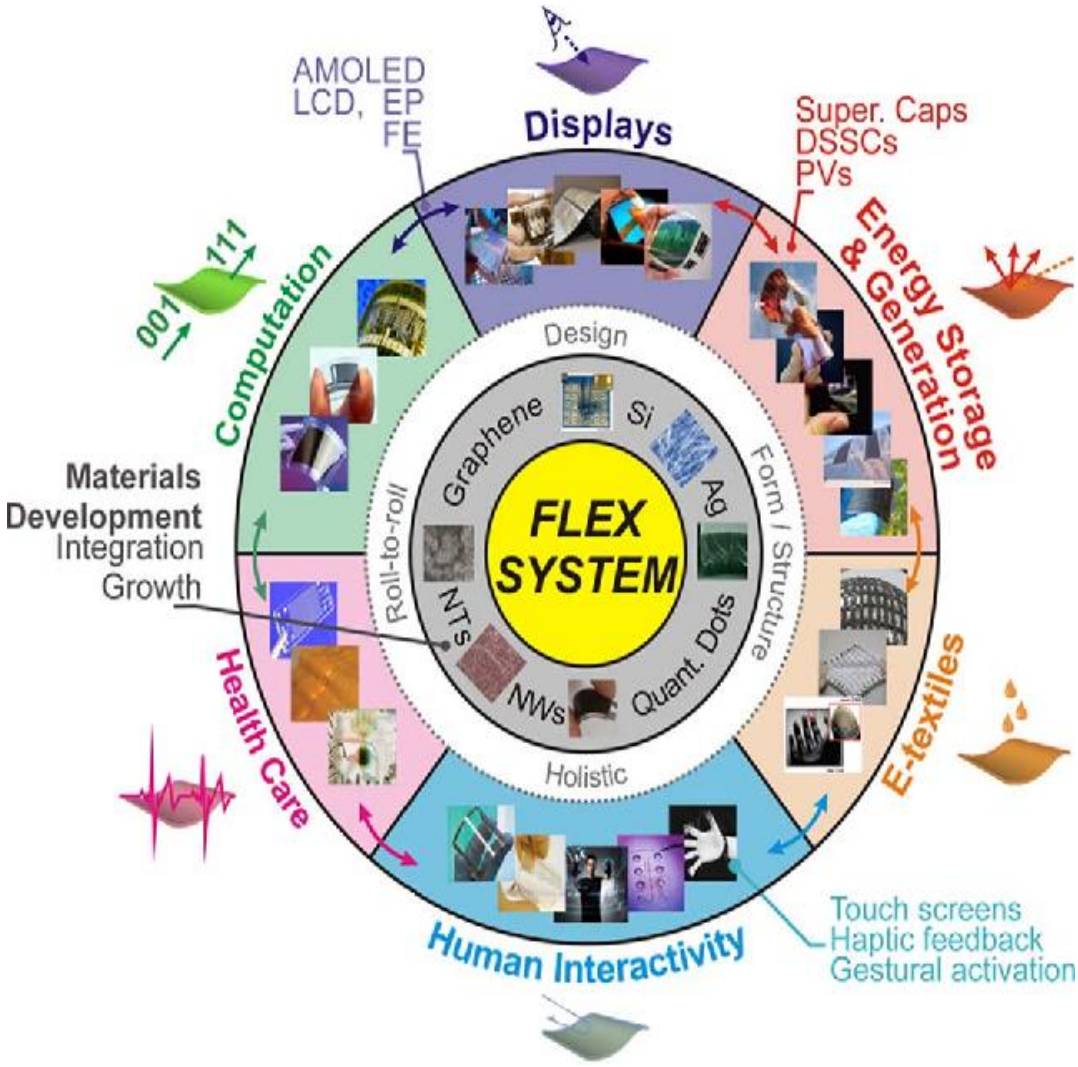

Fig 7: Applications of flexible electronics [34]

1.6 NANO-FABRICATION TECHNIQUES FOR FLEXIBLE ELECTRONICS:

These electronics usually consist of thin films which have a flexibility factor so the fabrication process allows the active materials to integrate on the soft substrate maintaining its electrical and mechanical properties.

Nano fabrication refers to the fabrication process under the dimension of 1 to 100 nm, the motivation of this is to miniaturize the device that benefitted in different ways.

- Reduce material cost
- Increase in the density of components
- Increase their performance; as a device and as integrated circuit

Nano fabrication requires lots of care in handling as a slight misalignment has a similar effect as the misalignment of the overlay of the mask [35].One of the main advantages of the flexible substrates is the roll-to-roll fabrication which has different methods of manufacturing the electronic devices as it combines both mechanical design as well as material process which makes it relatively more complex than the other techniques. Vacuum deposition in the layer-to-layer deposition is used for the solar cell as it is suitable for the layers required for a-Si:H TFTs [36].

Fabrication techniques on the flexible substrate constrains one to use the method having low processing temperature as high temperature can cause cracking, bubbling and oxidation might occur. The processing of the device can be effected by the exposure to the radiation and high temperature.

In order to focus on confining the device in the minimum possible cross-section with maximum sensing capabilities, one must use nanofabrication techniques. There are two approaches for the fabrication of flexible electronics.

- Top down
- Bottom up

Bottom up is a different approach for fabrication where we combine materials to form structure used as products or materials while we utilize top down approach in this work.

Top-down:

The conversion of bulk material into desired structure is named as top-down approach. In this approach, the dimension ranges from tens of nanometer to millimeter scale which propagates through conventional lithographic, deposition and etching techniques.

Printing technologies are further expressed into categories

i. **Contact Printing**

   Where there is a direct contact with the printing source and substrate. The amount of material wastage is high with limitations in resolution factor and

material range causing the printing technology to become more expensive and less accurate feature size.

Examples include Soft lithography, Nano imprint lithography, etc.

ii. Non-Contact Printing

In this printing technique, only deposited material is in contact with the material.

Examples include Laser Printing, Inkjet Printing, etc.

The material needs to be functionalized differently to take into account both mechanical and electrical attributes. Functionality causes variation in the use of the material with a little change in functional group. Integrating these functionalized materials onto the flexible substrate where both have the same young modulus results in good flexibility and avoid buckling. Laser writing method can also be used to draw conductive patterns onto graphene oxide.

1.6.1 LITHOGRAPHY:

It represents the process of transferring the image or circuitry onto the substrate in the more precise way usually in nano and micro size structures. These devices were then named as NEMS and MEMS devices. Unlike normal printing methods, its feature size is very precise. Lithography can be done by using light, ion beam or electron beam.

- Photolithography:

As shown by the name this lithographic technique utilizes photons of light to draw a pattern. A photo mask is used to draw a pattern onto the photoresist. Before exposing to light a photoresist layer is cast onto the substrate this photo resist is of two types either positive or negative according to the type of the material and the pattern we want to achieve. After exposing it to the UV light through the mask it softens (positive) or it hardens (negative) up the photoresist. In micro electroforming the most commonly used negative photoresist is SU-8 [37, 38] and positive photoresists are AZ4620, AZ1500 [38].

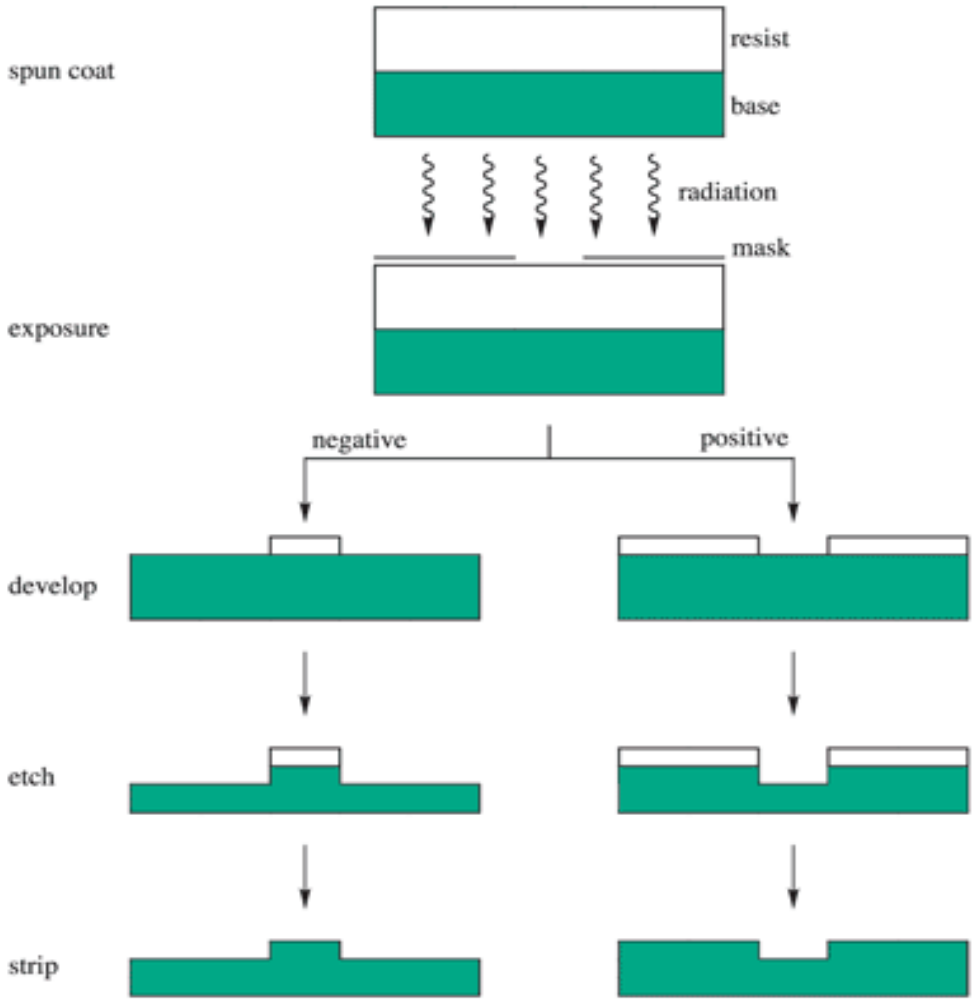

Fig 8: Photolithography for positive and negative tone resist and subsequent pattern transfer by etching.[39]

The more soft part, unexposed area in case of negative photoresist and the exposed area in case of positive photoresist is removed by the development process as shown in the figure. This patterned photoresist acts as the template for the substrate material etching is done to draw out the pattern on the material and then photoresist is removed. This technique is used for mass production in the industry because of the parallel writing capability. Multiple patterns can also be made by doing the same steps again.

- Scanning Beam Lithography

This technique falls in non-contact printing which doesn't need any mask to pattern but require beam of light or electrons to make changes in the resist for the formation of pattern.

1. **Electron Beam Lithography**

   A focused beam of electrons is used to draw patterns on the photoresist. Some commonly used resist materials are hydrogen silsesquioxane (HSQ), poly (methyl methacrylate) (PMMA), NaCl, ZEP, SiO_2 or LiF [40]. This technique is termed as EBL with minimum resolution size less than 10 nm which is better than any contact printing technologies. This techniques is used to draw below 500nm feature sizes[40].

2. **Ion Beam Lithography**

   This technique uses a very focused ion beam of He^+, Ga^+ or H^+ to draw patterns on polymer substrate. The chief advantage of ion beam lithography is less back scattering causing the proximity effect to decrease. Due to their heavier mass ions do not scatter upon interaction which helps getting better resolution than EBM.

3. **Optical Beam Lithography:**

   A mask less lithography technique used to produce pattern of precise shape and size. UV light is used to etch the resist according to the type of the resistance etching can be more or less. Feature size up to 50nm can be achieved depending upon the type of resist [41] manipulation in intensity and focal point of the beam can be able to control the height of the structure.

Fabrication method	Material complexity	Resolution	Total size	Geometric diversity	Materials diversity	Throughput
Photolithography	Multiple materials possible	Down to 37 nm;[83] potentially sub-10 nm[87]	15 cm diameter circular substrates	Two tunable dimensions	Only photosensitive materials	Very high
Scanning beam lithography: Optical beam lithography (OBL)	Single material structures	52 nm[34]	2 × 2 cm^2 substrates[45]	Three tunable dimensions	Only photosensitive materials	Low
Scanning beam lithography: Ion beam lithography (IBL)	Single material structures	8 nm[107]	12.5 × 12.5 mm^2 pillar arrays;[90] centimeter-sized patterns[105]	Two tunable dimensions	Polymeric or metallic materials	Low
Scanning beam lithography: Electron beam lithography (EBL)	Single material structures	4 nm[104]	Wafers and photomasks up to around 30 cm diameter[78]	Two tunable dimensions	Polymeric or metallic materials	Low

Fig 9: Comparison among photolithography, optical beam lithography, ion beam lithography and electron beam lithography. [42]

1.6.2 NANO FABRICATION BY MOLDING AND EMBOSSING

A number of fabrication techniques has been introduced to fabricate the micro and nano structure devices which usually require a proper environment and clean room unless this technique uses molds to transfer pattern results in high resolution without requiring any specific condition. This comes in the category of low cost fabrication techniques. We divide these techniques into two categories:

i. Molding and embossing with hard stamp
ii. Molding and embossing with soft stamp

A 3D mold is used to impress pattern on the resist which is already attached to the material. Hard molds are usually formulated by quartz and silica due to their inert behavior towards most monomers and pre-polymers and with temperature resistant ability ease the cross linking of polymers. That can be able to sustain nano scale features with minute distortion due to pressure [43]. The through-put is approximately 10-4 m^2 h^{-1} which is comparable to any serial writing technique [44]. Soft molds include a variety of polymer materials but PDMS is the most promising one used. This polymer is durable and chemically inactive to most of the material widely used. Low surface free energy (21.6 dynes/cm^2) [45], caused the mold not to attach with the resist that so that it does not break the feature. That can be further categorized into three kinds [43].

1. Nano imprint lithography
2. Embossing
3. Molding

➢ Nano imprint lithography:

This technique uses the hard mold to draw pattern onto the resist which have been heated to its glass transition temperature normally called as hot embossing [46]. When polymer hardens and the mold is separated it results in a good feature size of about ~5 nm [47, 48]. Throughput of NIL is really high if we use rolling pin that was first introduce in 2008 called R2RNIL (roll-to-roll nano-imprint lithography) [49].

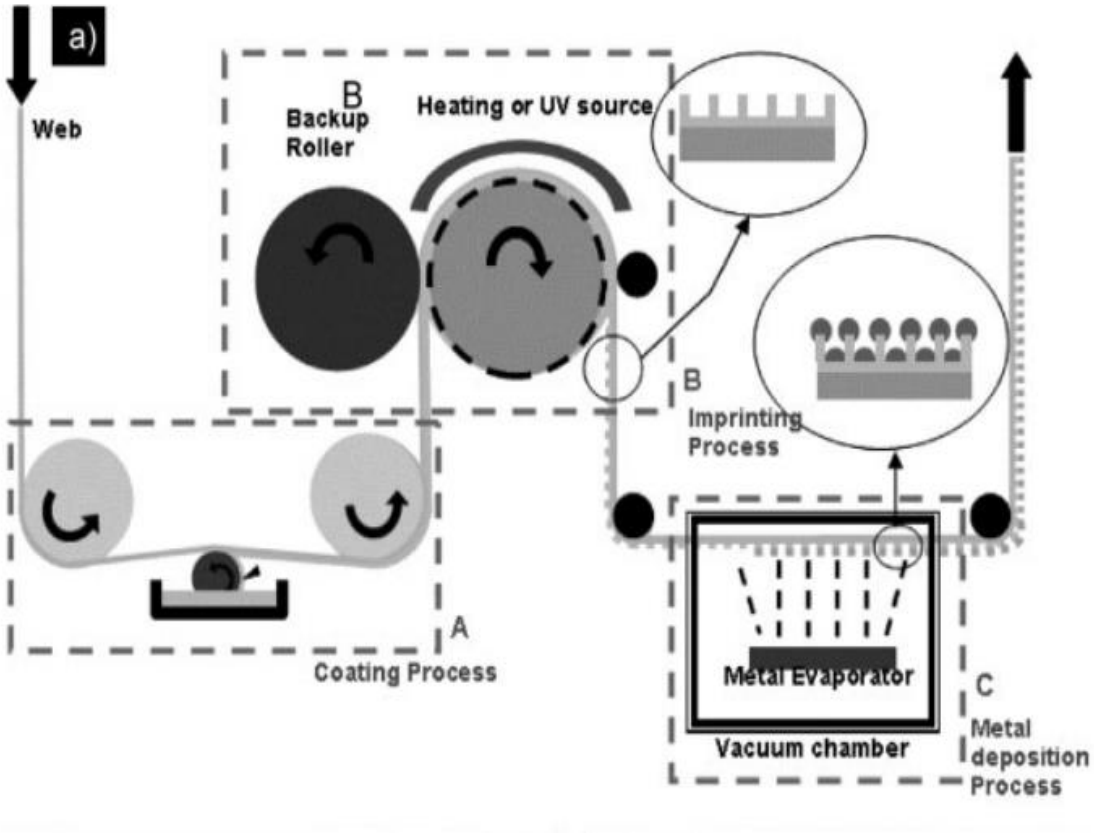

Fig 10: Working of roll-to-roll nano-imprint lithography [47]

1.6.3 ADDITIVE WRITING:

➢ Laser scribing:

Laser scribing is a serial writing technique which promises to attain the feature sizes of few microns without need of any vacuum environment or clean room. This technique is not only simple but requires less time and the device itself costs very less which makes this a good candidate for mass production. Laser can be used in two ways:

- By focusing the laser to one point and scanning over the surface to draw the desire shape.
- By projecting the mask having patterned image in between surface and laser to draw patterns.

This fabrication technique uses a focused beam of light to draw a pattern on the substrate which has been provided by laser software driven by the instructions from

the computer. In this technique Nd:YAG, CO^2, UV, excimer or pulsed laser can be used to alter the composition, morphological structure or chemical structure of the substrate at room temperature [50]. A facile approach restricted to few materials including graphene oxide GO, polyimide PI, polydimethylsiloxane PDMS, polyethylene terephthalate (PET) etc. In this approach, the surface morphologies are changed at higher temperatures by photo-chemical and photo-thermal irradiation causing the reduction of the material [51]. This results in the removal of some functional groups present rendering the area to be relatively more conductive. Almost no chemical contamination occurs, which also makes this method environmentally friendly as compared to optical lithography where the developer and solvents must ultimately be disposed.

- *Regions of laser interaction with material:*

In terms of the response of the material, three regions can be defined:

- Growth region:
  Laser power of this region is 1-60mW. Graphene oxide is converted into reduced graphene oxide (RGO) and an increase in the thickness of the material due to the gasification of oxygen containing functional groups is witnessed.
- Transition region:

  Transition region range utilizes the power of 60-180mW. Growth of the material takes place but also etching occurs at the same time. This makes it a different region where the thickness of the material remains the same.
- Etching region:

  High power more than 180mW causes the material to etch away leaving behind channels or pathways reducing the thickness of the material.

Laser engraver consists of a stage that can be moved in X and Y direction on which a sample has been put to fabricate the pattern. To draw a pattern onto the substrate a picture has been made on Adobe Illustrator and uploaded on the laser software. Laser beam was firstly focused to draw any pattern to achieve high resolution.

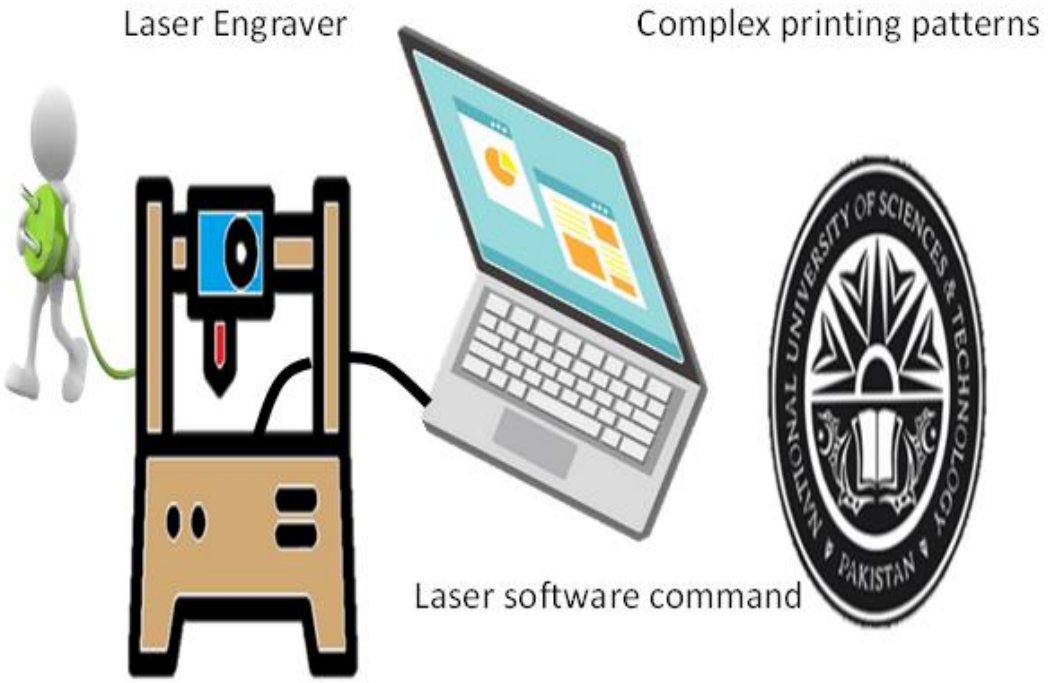

Fig 11: Laser engraver connected to the laptop for instruction to scribe pattern as NUST logo to scribe.

1.7 SUBSTRATES FOR FLEXIBLE ELECTRONICS:

There are three kinds of substrates used for flexible electronics.

i. Metals
ii. Plastics
iii. Flexible glass

1.7.1 PROPERTIES OF THE SUBSTRATE:

Flexible substrates should own these properties.

i. **Optical transparency:** Transparent and Flexible LCD substrates require optical transparency.
ii. **Surface roughness:** Most metals have lots of roughness while plastics have roughness over a long period. Polishing can help to reduce the surface roughness [52].
iii. **Thermal and thermo mechanical properties:** Material must have temperature resistance if it has been processed at the glass transition temperature (*T*g). The coefficient of thermal expansion CTE mismatch of the

layers can lower the device lifetime and cause the breakage of the substrates while device is in a working state. Low CTE based silicon substrates are beneficial for that but thermal stability is a concern in the case of plastic substrates.

iv. **Chemical stability**: The substrate should be chemically stable towards the process and must not release any kind of toxic gases that affect the stability of the device.

v. **Mechanical properties:** Low elastic modulus promotes flexibility and high elastic modulus reflects the stiffness.

1.7.2 METALS:

Metals can also be flexible if it is under the thickness of ~125μm. Metals are popular in devices which do not require any optical transparency. Very few metals are used when flexibility factor comes under consideration. Stainless steel is best for this because of its resistance towards corrosion and it is highly durable as well. Silicon substrates are also popular due to their low CTE.

1.7.3 THIN GLASS:

Thin glass substrates are mostly used in flat panel displays due to their optical transparency when thickness is less than 30μm and they have become flexible. Thickness under few 100μm, surface roughness of 1nm, low CTE, temperature resistant up to 600◦C, high dimensional stability makes it a perfect candidate. Due to their brittleness they can be easily breakable to increase their stability: they are overlaid with a thin layer of polymers or often encapsulated in plastic foil.

1.7.4 ORGANIC POLYMER:

Organic polymers are flexible and very inexpensive compared to similar materials. They also promote roll-to-roll fabrication [25], which results in high throughput [53]. Glass transition temperature is very important due to which they are thermally unstable as their operating temperature is much less than the thin glass. However they are dimensionally unstable as well and the molecules expand isotropically as long as the glass transition temperature is not achieved [54] and also water and oxygen are easily permeable by them that can affect the T_g. High glass transition temperature,

low coefficient of thermal expansion CTE is important. Organic polymers are usually expressed into three categories[25]:

i. Thermoplastic semi-crystalline polymer: These comprise of the polyethylene terephthalate (PET), polyethylene naphthalate (PEN) and polydimethylsiloxane (PDMS) [55].
ii. Thermoplastic non-crystalline polymer: Polycarbonate (PC) and polyethersulphone (PES) are examples of this category.
iii. High-Glass transition temperature materials: Examples include polyarylates (PAR) and polyimide (PI).

PC, PES, PDMS and PAR show transparency that have high CTE and PC, PES, and PAR have high T_g then PET and PEN. PET and PI as well as PEN have relatively small CTE and have good resistance to the chemicals.

Table I: Properties of typical materials for 100-µm-thick foils [56-58]

Property	**Unit**	**Stainless Steel (430)**	**Glass (1737)**	**Plastics (PI, PEN)**
Thickness	µm	100	100	100
Weight	g/m^2	800	250	120
Roll-to-roll processable?	–	Yes	Unlikely	Likely
Safe bending radius	Cm	4	40	4
Visually transparent?	–	No	Yes	Some
Elastic modulus	GPa	200	70	5
Maximum process temperature	◦C	1,000	600	180, 300
CTE	ppm/◦C	10	4	16
Permeable to oxygen, water vapor		No	No	Yes
Prebake required?	–	No	Maybe	Yes

Buffer layer required? Why?	–	yes: electrical insulator, chemical passivation	Maybe	yes: adhesion, chemical passivation
Electrical conductivity	–	High	None	None
Thermal conductivity	W/m·◦C	16	1	0.1–0.2
Deform after device fabrication	–	No	No	Yes
Planarization required?	–	Yes	No	No

- Polydimethylsiloxane (PDMS):

PDMS is famous for its biocompatibility and flexibility consisting of a trait of six degree of freedom which constraints of three categories.

i. Bending (up, down)
ii. Stretching/compression
iii. Torsion (clockwise, anti-clockwise)

PDMS is available from Dow Corning Corporation as Sylgard ® _ 184 appears to be available in two different solutions pre-polymer (base) and cross-linker (curing agent) that combine together to form layer [59].

- Production of PDMS:

It is one of the multipurpose materials which can be used for different application to make mechanically stable and flexible devices as a packing material or as a substrate. Micro structuring of PDMS causes the improvement in sensitivity specifically for pressure sensing application.

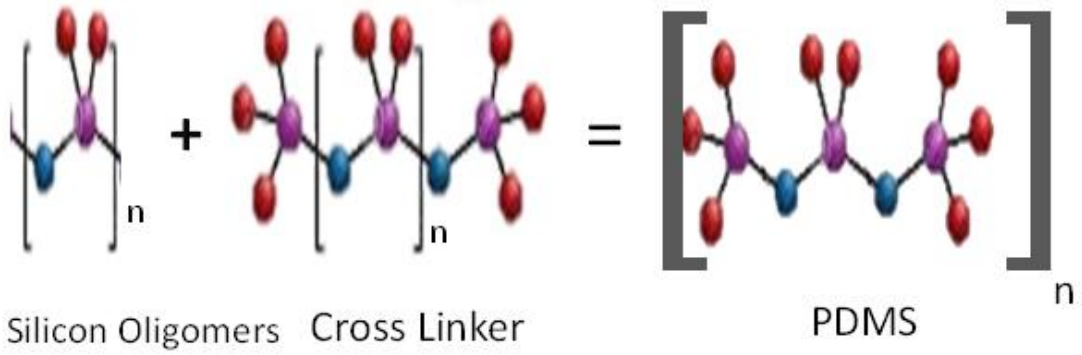

Fig 12: Chemical process for curing polydimethylsiloxane (PDMS)

Microstructures allow elastic deformation for external force applications so consequently storing and releasing the energy will lead to minimizing viscoelasticity [60]. Mechanically stable PDMS have young's modulus of 1.8MPa [61-63]. It is really very cheap compared to glass. Insulating property of PDMS allows them to use as the insulating layers around them.

Table II: Some relevant characteristics of PDMS (Sylgard 184, 1:10 catalyst to base polymer). [51]

Characteristic	**Value**	**References**
Optical transparency	240–1100 nm	[42, 43]
Surface tension	21–22 mN/m	[44]
Glass transition temperature	−125 ◦C	[44]
Electrical conductivity	2.9 E + 14 _S/cm	[45]
Heat conductivity	0.27 W/m*K	[45]
Young's elastic modulus	E ∼1–3 MPa	[46, 47]
Surface tension	21 mN/m	[44]
Water vapor diffusion	∼1000–6000 _m^2 s^{-1}	[48]
Oxygen diffusion coefficient	∼2000–4000 _m^2 s^{-1}	[49]
CO_2 diffusion coefficient	∼1000 _m^2 s^{-1}	[50]

1.8 SENSING MATERIALS:

Two-dimensional materials and their derivatives have attracted lots of attention towards their use as active materials due to their physical and chemical properties. For example, graphene shows very good conductivity, flexibility and partial transparency when used in layer form. CNT is also a very good conductor. There are many metals like Ag that are used as an active material for making devices. Hydrogels are also providing very good sensitivity and flexibility[64].

1.8.1 GRAPHENE OXIDE AND REDUCED GRAPHENE OXIDE:

Structure: A unique material that consists of the single monochromatic sheet of graphite. It is an sp2 hybridized atom consists of ring base hexagonal structure that also have partially sp3 hybridized atom having oxygen containing functional groups e.g., carboxyl, hydroxyl and carbonyl groups.

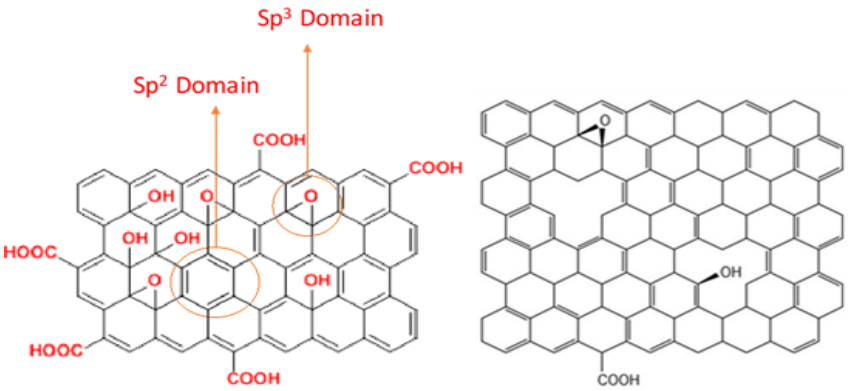

Fig 13: Conversion of GO (left) into RGO (right)

GO is formed by oxidizing the graphite that creates interlayer spacing causing the layers to separate out and form a monolayer. That process results in functional groups attachment. Due to the presence of functional groups the sp2 hybridized atoms are in disruption therefore GO exhibits the insulating property [65]. Functional group also reduces its elasticity [66]. RGO is formed by the reduction of GO. Reduction cause the oxide group to leave the GO by chemical , photo thermal, photo chemical, thermal [67], microwave and microbial methods to minimize oxygen level.

i. Synthesis:

Hummer's method is the most commonly used method to produce GO. This method exfoliates the graphite solution by potassium permanganate. Sodium nitrate and sulphuric acid are mostly used to naturally exfoliate the graphite sheets that are separated out by surface polarity. There are other modified versions of the Hummer's method used to synthesize GO shown in fig 14.

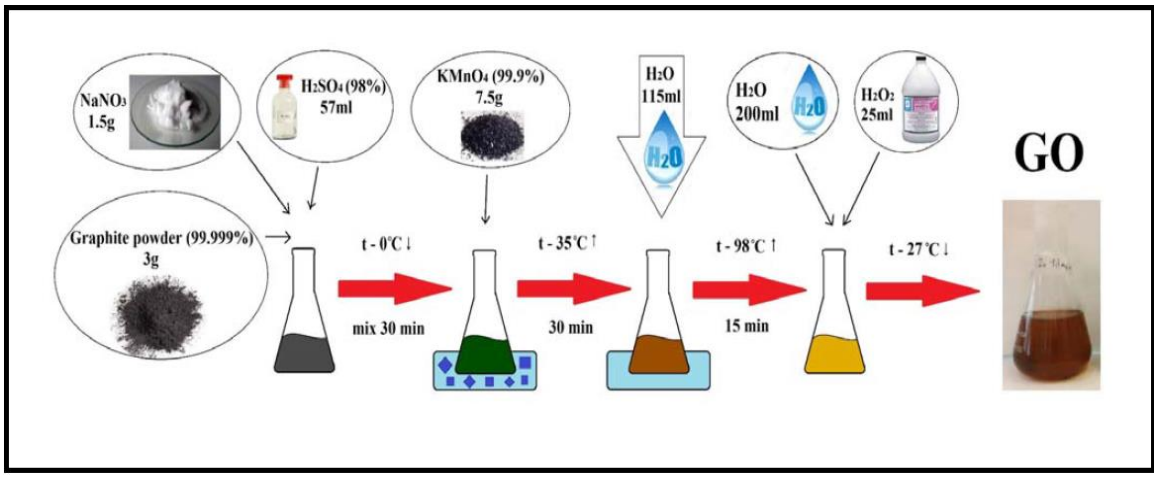

Fig 14: Production of GO by Modified Hummer's method[68]

ii. Properties:

GO reportedly has low electrical and thermal conductivity due to the presence of oxide groups in contrast with the reduced graphene oxide having high conductivity. The conductivity of the RGO depends upon the reducing agent and the reduction route. Chemical structure and properties differ by using hydrazine hydrate (HH), hydro-bromic acid (HBr) and hydroiodic (HI) acid as a reducing agent. Conductivity is amplified by a considerable amount of using HH and HI reducing agents for prolonged time period [69].

Table III: Electrical and mechanical properties of GO and RGO

	GO	RGO	Reference
Conductivity	Non conductive	~667 S/m***	[70],[71]
Younge's modulus	380-470 GPa*	250±150 GPa**	[72], [70]/[73]
Water solubility	Highly dispersible	Moderately dispersible	[70]
Transparency	23–77%		
Density		$1.91 g/cm^3$	[71]
Humidity	15%–95%	3.7 - 4.2%	[74],[71]
BET surface area	$\sim 240 \pm 59\ m^2\ g^{-1}$	$422.69 – 499.85 m^2/g$	[75],[71]

CHAPTER 2: LITERATURE REVIEW

2.1 FLEXIBLE TECHNOLOGY:

Flexible pressure sensor technology has attracted a lot of attention due to their wide application areas, enhancement of efficiency in our day-to-day lives and ability for real time monitoring [27, 28, 30, 31, 76]. There are a lot of work that had already done to specifically monitor health like heartbeat, blood pressure, eye pressure, therapeutics[28], breathing issues and speech recognition[28]. These flexible sensors can be set up on wearable electronics which provides real time health monitoring of persons suffering from diabetes or blood pressure, on clothes (which cover almost 90% of the body), and also work as electronic skin[28, 76] which can be used in prosthetics and on the burnt area of the body.

Here the flexibility factor provides a better opportunity to bend and stretch and form any structure. Due to this property, electronic devices can be mounted anywhere on the human skin and clothes and on the bandages for wound monitoring. Flexibility is a property of polymers which not only provides good performance but also make them light weight and easy to carry. Polymers not only provide flexibility but also help in providing good contact with the skin. Most of them have the ability to stick to the skin due to the elastic moduli of the polymer which is much closer to the biological tissues.

In literature we have found many applications for flexible materials not only they show flexibility but also have good mechanical properties. There are a lot of publications on the packaging of food items because of their variable properties, e.g., some of them have good permeability of air, and some of which create the barrier for oxygen and moisture which would be required according to the packaged material. Flexible materials are also used for the packaging of electronic devices to increase their lifetime. It is used in integrated circuits

Flexible organic light emitting devices are also reported in the literature. Flexible displays are attracting a lot of attention these days. There are also some of the companies that are working on mass production. Including previous work flexible solar panels were also introduced that are mounted on the fiber clothes that can be

easily foldable and easy to carry. Flexibility also plays very important part in making energy storage devices like super capacitors circuits and batteries which helps in making flexible electronics like flexible displays, watches, etc.

2.2 STRAIN SENSOR:

There are a variety of materials that have been used to fabricate strain sensor. Two most widely used materials are CNTs [77-79] and graphene materials with structural and chemical differences[80-88]. These graphene materials include GO/RGO [81], graphene [82, 89], LSG[83], few layer graphene [80], graphene nano platelets [84], hollow tubing graphene fibers (TGFs) [85], carbon nanocoils (CNCs) [86], carbon nanostructures (CNS)[87], electro-conductive carbon black nanoparticles [88], three-dimensional graphene foam [90], graphite glue [91], and molybdenum-carbide-graphene(MCG) [92]. Other than graphene, conductive polymers are also good electrically active materials when it comes to sensing like PI [83] which turns conductive after laser scribing. Polymers contains a very good property of flexibility that make them a good substrate as well [93]. Polydimethylsiloxane (PDMS) is not only a perfect candidate for substrate [78, 79, 85, 90, 94, 95] but also a distinguished conductive material after reduction [96] due to its skin like flexibility and natural movements with skin [97] and high optical transparency it can be used as alternative skin which is also called electronic skin number of researches had already been done on this area [98-100] which used in soft robotics [101]. Flexibility of PDMS base sensors depends upon sensing components and their hydrophilicity. PDMS itself is a hydrophobic material that is converted into hydrophilic to increase its adhesion with the sensing material by using different methods such as Ultraviolet–ozone treatment [79] plasma etching and CO_2 plasma treatment[102]. Although PDMS based strain sensors are competent in measuring 280% strain [77]. Mostly PDMS is used as the base to provide flexibility. Anyhow sometimes it can be used to sandwich the materials for securing the device from buckling.

Strain sensors are further divided into four categories depending upon their mechanism. Piezoresistive, piezocapacitive, piezoelectric/piezotronic, Impedance and Triboelectric [103].

The sensing region falls in two categories according to the limit of the strain.

- Large scale detection

Human motion detection, arm movement etc.

- Small scale detection

Heartbeat, blood pressure measurement etc.

2.2.1 REQUIREMENTS OF FLEXIBLE STRAIN SENSOR:

- High sensitivity (gauge factor)
- Fast response time
- Durability
- Consistency
- Good Flexibility
- Low cost
- Convenient

Recently everyone is working on making the device which is more convenient, have good sensitivity and fast response.

2.2.2 PIEZORESISTIVE TYPE STRAIN SENSOR:

Piezoresistive is the sensing mechanism through which a sensor works. Medium of sensitivity is the change in resistance of the material caused by physical strain. Resistivity of the sensor changes to highest or the lowest. The higher the resistivity changes, the maximum the gauge factor. Strain sensors work for two ranges, i.e., a higher strain range and lower strain range depending on their fabrication process [78, 81-84, 89, 91, 92, 95, 104]. These strain sensors can be used to make devices whose purpose is to measure smaller value ranges e.g., pulse measurement, human vocal vibration detection when speaking [105, 106], etc. Mulberry paper shows a gauge factor of 3.82 and is utilized to form wearable sensors [78, 104]. The maximum range a sensor can measure depends upon sensing material's stretchability, although the maximum strain that has been observed in polymer is 450% where hydrogels show two regions and their different gauge factor. Sensitivity ranges 0-300% and 300-450% have guage factors of 2.9 and 7.4, respectively. Silver nanowire elastomer strain sensor shows elevated amount of strain range up to 70% with a presentable gauge factor range of 2-14, which is used for the detection of finger joint movement [107]. Conductive silver ink and silicone elastomers combine together to show higher range

of strain up to 75% with gauge factor of less than 104 to 106 which make this material to use in muscle motion detection [108]. A conductive polymer named poly(3,4-ethylenedioxythiophene) polystyrene sulfonate (PEDOT:PSS) microchannel shows top notch gauge factor of 12000 [94] among other conductive polymers. Indium tin oxide (ITO) is considered to be a very good material for LCD displays and touch panels. Due to its transparency, it proves its credibility in measuring small movements in strain sensors as well. It can detect 0.24% to 0.92% strain for tensile and -0.99% to -0.24% for compressive type strain having gauge factors of 41.98 and 21.36 respectively [109]. CNT and their structures are also very promising materials for strain sensing. The maximum noted strain range for carbon nanotubes (CNTs) is 150% for the gauge factor of 0.05 used for speech recognition and breathing measurement [77]. Interlocked microdome arrays of MWCNTs combined with PDMS is a really promising combination to calculate high strain range of 100%-120% and also uplift the standard for CNTs based strain sensors by showing a gauge factor of 9,617 [110]. Paper-based MWCNTs are also good for measuring low range strain of 0.098% having GF of 263.34 [78]. Researchers are working on materials which are not only cost effective but smart enough to be easily handled and can also be mounted on skin or have skin like structure for convenient and live measurement of health care issues like cardiac eye glaucoma etc. Researchers are collaborating towards the development of multipurpose flexible devices.

2.2.2.1 Graphene piezoresistive strain sensors:

Graphene is a very promising material for sensing due to its high conductivity and good mechanical properties. A study in 2014 found elastic bands pervaded with graphene showed the gauge factor of 36 with a stretchability of 800% which is highest among all other materials including graphene [106]. While the highest gauge factor observed is 10^6 by extremely thin sheets of graphene woven fabrics. This GF was observed due to the presence of good van der Waals Forces between the graphene and PDMS with the sheet resistance of 400–500 Ω sq^{-1} [82]. The desirable GF can also be obtained by changing the concentration of graphene flakes in graphene PDMS composites. At the concentration of 8.33 vol.%, the GF is 233 at 2% strain [89]. Some strain sensors can be observed as having high GF with low strain range as RGO and PI composite fabricated by using low cost method of laser scribing having GF of 54.2

at 0.003% strain elucidate this as a very sensitive sensor towards the small movements [83] while another reduced form of graphene on fibers evinced the strain range of 5% with GF of 8.8 [81]. The definition of perfect strain sensor fits on poly(styrene-butadienestyrene)/few layer graphene composites strain sensor which shows significant amount of strain range 100% due to the good interfacial π-π interaction between graphene and phenyl group of SBS causing gauge factor of 2,546 [80]. To increase the sensitivity, graphene was prepared by changing the physical structure of the graphene to braided graphene belts. Their structure makes this sensor highly flexible that can stretch and bend and shows good GF of 175.16 at 55.55% strain making it a good candidate for monitoring body movements [95]. Some piezoresistive materials and their properties are mentioned in the table below:

Table IV: Different properties of piezoresistive strain sensor.

Active Materials	Sensing Mechanism	Flexibility/ Strain range	Gauge factor	Device Applications	Year	Ref
Graphene, polydimethylsiloxane (PDMS)	Piezoresistive	2%.	233	Strain sensor	2013	[89]
RGO coated elastic fibers	Piezoresistive	5%	8.8	Smart clothing	2017	[81]
Interlocked microdome arrays[multi-walled carbon nanotubes (MWCNTs), polydimethylsiloxane (PDMS)]	Piezoresistive	90–120%.	9617	Pressure, Shear, Strain, Curvature of Electronic skin	2014	[110]
Graphene Woven fabrics, polydimethylsiloxane (PDMS)-tape	Piezoresistive	>7%	10^6	Displays, Robotics, Fatigue detection, Body monitoring	2014	[82]
Laser scribed GO, PI hybrid	Piezoresistive	0.003%	54.2	Strain sensor	2018	[83]

Silver Nanowire_Elastomer	Piezoresistive	70%	2-14	Motion detection of fingers	2014	[107]
Stretchable Carbon Nanotube (CNTs)	Piezoresistive	150%	0.05	Typing, Breathing, Speech	2011	[77]
Poly(styrene-butadienestyrene)/few layer graphene(SBS/FLG)	Piezoresistive	100%	2546		2018	[80]
Paper, multi-walled carbon nanotube (MWCNTs), polydimethylsiloxane (PDMS)	Piezoresistive	0.098%	263.34	Wearable electronics, Water environmental protection, Underwater robots.		[78]
Mulberry paper, graphene solution	Piezoresistive	0.587%	3.82	Wearable strain sensor	2020	[104]
Conductive silver ink, nylon fabrics, silicone elastomer	Piezoresistive	75%	>104–106	Muscle movements	2018	[108]
Graphene nanoplatelets, polyester fabric	Piezoresistive	5%	30	Smart clothes, Respiration, Heart rate	2021	[84]
Hollow tubing graphene fibers (TGFs), polydimethylsiloxane (PDMS)	Piezoresistive	8%	34.3–48.9	Finger joint motion	2017	[85]
Conductive polymer PEDOT:PSS, polydimethylsiloxane (PDMS)	Piezoresistive	10%	12 000	Control a robotic finger movement using human hand	2020	[94]
Braided Graphene Belts	Piezoresistive	55.55%	> 175.16	monitoring human motions	2020	[95]

Carbon nanocoils (CNCs), poly(3,4-ethylenedioxythiophene):poly(styrenesulfonate) (PEDOT:PSS)	Piezoresistive	50%	25	Wearable healthcare devices , E-skins	2021	[86]
Carbon nanostructures (CNS), Purified psyllium husk (Psy), polydimethylsiloxane (PDMS)	Piezoresistive	20%	4.5	Compressible switches, Human motion detection	2021	[87]
Three-Dimensional Graphene Foam/ Polydimethylsiloxane (PDMS)	Piezoresistive	15%	6.24	Real-time monitoring of Buildings, Bridge, Dam, and High-speed railway.	2014	[90]
Graphite glue, paper	Piezoresistive	0.495%	804.9	Structural monitoring system, Wearable smart devices, Intelligent visual system	2013	[91]
Molybdenum-Carbide-Graphene(MCG), paper	Piezoresistive	0.07% to 0.25%	73(tension), 43(compression)	Human body motions	2020	[92]
Aqueous single-walled carbon nanotube (SWCNT), Polydimethylsiloxane (PDMS)	Piezoresistive	80%	2.75	Dynamic hand motions	2019	[79]

Conductive titanium carbide nanosheet (MXene), polyurethane/polyacrylonitrile	Piezoresistive	80%	9.69	Electronic skins, Smart robotics, Biomedical monitoring and motion detection	2021	[105]
Conducting hydrogel	Piezoresistive	0-300% 300-450%	2.9, 7.4	Bending/vibration deformations	2021	[64]
ITO Nanoparticle channels, Polydimethylsiloxane (PDMS)	Piezoresistive	0.24%to0.92%(tensile) -0.29%to-0.99%. (compressive)	41.98(tensile)21.36 (compressive)	Weak motion monitoring of humans and robots	2019	[109]
Graphene-infiltrated Elastic bands	Piezoresistive	800%	36	Finger, hand and throat movement, Breathing, Speaking words	2014	[106]

2.2.3 PIEZOCAPACITIVE AND PIEZOELECTRIC MATERIALS:

Piezocapacitive materials are good for measuring smaller movements while the piezoelectric materials are known for high GF. Some of the materials are mentioned in the table below.

Table V: Properties of piezocapacitive and piezoelectric strain sensor

Active Materials	Sensing Mechanism	Flexibility/ Strain range	Gauge factor	Device Applications	Year	Ref
Copper, polyimide(PI), epoxy resin	Piezocapacitive	1.25%	-0.75	Automobile radial tire	2007	[93]

Lead–zirconate–titanate _PZT. and polyvinylidene fluoride _PVDF.	Piezocapacitive	0.0275 % & 0.033%	6 & 3.5		1999	[111]
Gold, silicon wafers (p-type)	piezocapacitive	0.1%	252	Spinal fusion application	2007	[112]
Electro-conductive carbon black nanoparticles, ethylene-propylene-diene monomer, Electro-conductive fabrics	Piezocapacitive	30 %	3.5	Civil structures monitoring	2021	[88]
n-ZnO/p-NiO heterojunction	Piezoelectric	0-1%	196	Breathing, Joint motions	2019	[113]
ZnSnO3 nanowires/microwires	Piezoelectric	0.32%	3740	Strain sensor	2012	[114]

2.3 GAUGE FACTOR:

Gauge factor is the measuring scale to calculate the sensitivity of the strain sensor. It will be calculated by the formula mentioned below.

$$G.F = \frac{(R-R^\circ)}{R^\circ\varepsilon}, \frac{(I-I^\circ)}{I^\circ\varepsilon}, \frac{(C-C^\circ)}{C^\circ\varepsilon} \text{ ——————(ii)}$$

This is the gauge factor for piezoresistive, piezoelectric and piezocapacitive material respectively and ε is the strain after applying any physical change. High sensitivity strain sensors have been obtained by enhancing the material properties and their mechanical properties either by functionalizing them or by making composites with other promising materials. Amalgamation of this with polymer materials adds up flexible properties to the device making it user friendly.

2.4 LASER SCRIBING:

Laser scribing is used for making different electric devices. Mostly used for reducing graphene oxide and partly making it conductive. The wide spread of this laser reduced graphene oxide starts from any type of sensor to super-capacitor, optoelectronic

devices, etc. [115]. The composites of laser reduced graphene with other materials are also use to enhance the property of electric device.

Table VI: Laser scribed materials and their applications.

Title	Material scribed	Application	Year	Ref
Ultrasensitive MWCNT/PDMS composite strain sensor fabricated by laser ablation process	Multi walled carbon nanotube(MWCNT)	Strain sensor	2020	[116]
Laser Fabrication of Graphene-Based Flexible Electronics	Graphene/ Graphene oxide/ graphene prepare from CVD	Power generators, supercapacitors, optoelectronic devices, sensors	2019	[115]
Black Phosphorus@Laser-Engraved Graphene Heterostructure-Based Temperature–Strain Hybridized Sensor for Electronic-Skin Applications	Laser-engraved graphene (LEG)	Temperature and strain	2020	[117]
Laser-Scribed *N*-Doped Graphene for Integrated Flexible Enzymatic Biofuel Cells	Laser-Scribed *N*-Doped Graphene (PI)	Biofuel cell	2020	[118]
PEDOT-modified laser-scribed graphene films as bginder– and metallic current collector–free electrodes for large-sized supercapacitors	polyimide (PI)	Electrodes for supercapacitors	2020	[119]
Fabrication of electrochromic devices by laser patterning of spin-sprayed transparent conductive Ga:ZnO films	SSedGZO film	Electrochromic devices (ECDs)	2020	[120]
Effects of laser scribed Mo groove shape on highly efficient Zn(O,S) based Cu(In,Ga)Se2 solar modules	groove shape Mo	Solar modules	2019	[121]
Fabrication of Low-Cost and Highly Sensitive Graphene-Based Pressure Sensors by Direct Laser Scribing Polydimethylsiloxane	Polydimethylsiloxane (PDMS)	Pressure sensor	2019	[96]

The main usage of laser scriber was only to reduce graphene oxide but in recent years it has been found that it can also be used to enhance conductivity of Multi walled carbon nanotubes (MWCNTs) [116]. Laser scribing creates patterns by engraving the SSedGZO(spin-sprayed Ga:ZnO) film. That film acts as the pattern to fabricate color Electrochromic devices (ECDs) displays [120]. Electrically inactive polymer materials also become active conductors after laser scribing e.g., polydimethyl siloxane (PDMS) is converted into graphene[96]. Applications of these types of materials are Biofuel cell and polyimide (PI) Electrodes for supercapacitors [122], Pressure sensors and electronic skin etc.

2.5 MOTIVATION:

Electronic skin is such a demanding area now-a-days which have a wide range of applications in the bio medical industry as the strain or pressure sensing devices and the real time monitoring of any serious health issue. Health monitoring devices also costs a lot less than normal and they are also very beneficial for the patient for providing the quick medication. The main part in electronic skin is the strain sensor while some other functions can also be added in the device e.g temperature measurement, sweat measurement, etc. It can also be very useful for the people with vocal and muscular issues and also nerve damage issues after any accident. The bio inspired electrical devices work best on these kinds of issues. Laser scribing technology is a very cheap method to fabricate the strain sensor which exhibits high sensitivity. PDMS is used with the conductive RGO engraved by laser for sensing a good amount of strain.

2.6 AIMS AND OBJECTIVES:

1. To integrate a device that makes use of low-cost fabrication method like laser and it is also less time consuming.
2. Utilize abundant and low-cost materials to fabricate the strain sensor.
3. To make a flexible strain sensor containing sixth degree of freedom.
4. To ensure that the device is sufficiently robust to avoid the calamities of field-work, transfer, etc.
5. Ability to attach with human skin and respond to muscle motion.

CHAPTER 3: METHODOLOGY

3.1 EXPERIMENTATION:

We have fabricated highly flexible strain sensor device using laser scribing method on graphene oxide (GO) and polydimethylsiloxane (PDMS) is also used to provide its flexibility. The strain sensor provides a very cheap fabrication process and the materials are also readily available.

3.1.1 MATERIALS:

Some requisite materials for this project are mentioned below:

- Graphene oxide (GO)
- Polydimethylsiloxane(PDMS)
- Copper Tape
- Silver paste
- Acetone
- Deionized (D.I) water

3.1.2 APPARATUS NEEDED FOR THE EXPERIMENTATION:

- Petri dish
- Beaker
- Spatula
- Measuring pipette
- Curved pointed tweezers

3.1.3 INSTRUMENTS:

Instruments that are used to proceed the experimentation of this project are mentioned below:

- OSRAM diode laser (λ = 450nm, near UV).
- JEOL Analytical SEM (JSM-6490A).
- RAMAN (BWS415-532S, USA)
- Strain Sensor Test Rig (custom made)
- STOE θ-θ XRD Diffractometer

- Bath Sonicator
- Electrochemical Workstation(VSP)

3.2 FABRICATION OF STRAIN SENSOR:

We have divided the fabrication of strain sensor into 3 steps:

3.2.1 THIN FILM PREPARATION:

GO was prepared locally by Modified Hummer's method. To cast the thin film, we firstly need to prepare a GO solution with D.I water in ratio 3:1, respectively, in the beaker. Bath Sonication of this solution has been done for 2.5 hours to agitate GO particles into water. Then this solution is drop-casted in a petri dish to make thin film. It takes almost 1 hour to dry this solution in the oven at 110˚C. Then the second material we use here is PDMS which consists of a cross-linker (curing agent) and pre-polymer (base) which are mixed in a ratio of 1:10 respectively [94, 123]. This PDMS mixture is drop casted onto already dried GO and air pressure is used to remove the bubbles from the mixture and let the PDMS dry in the oven for almost 120 minutes at 80 ˚C [124]. This layer was then flipped upside down after drying. The purpose of preparing the GO layer first and then pouring the liquid PDMS after is that to increase the adhesion of both layers with each other. The liquid PDMS penetrates in between the layers of GO by using porous structure that cause the increase in mechanical bonding [107]. The hydrophobic property of PDMS makes it really difficult to attach with the GO layer. This preparation method is to avoid delamination between layers.

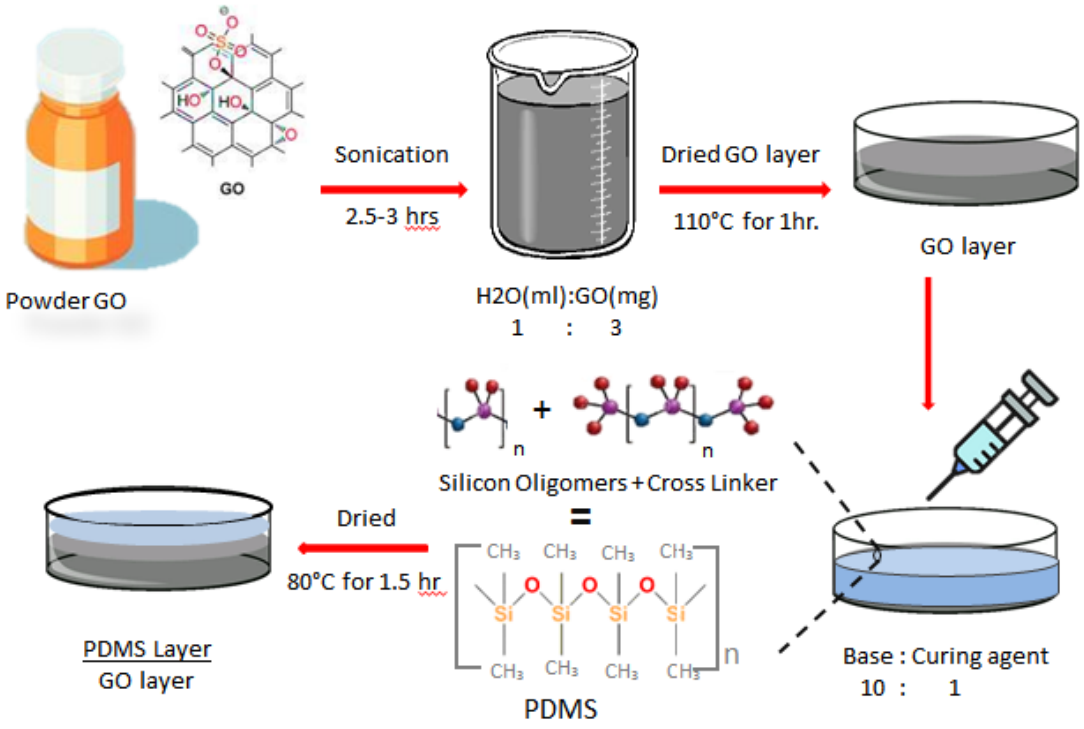

Fig 15: Synthesis process of initial fabrication of the device

3.2.2 LASER FABRICATION ON GO

Next step is to draw a pattern. In this experiment we are converting insulating material into conductive by laser irradiation using a laser engraver device. Laser engraver works by connecting to a laptop or a computer. The picture of laser engraver and the software is attached in Fig. 16.

An image of 1×1 cm with two poles has been prepared with respect to the pixels with high accuracy and saved as a BMP image. The command to pattern the image has been given to the laser engraver by software. Thin layer was then put on the stage of the laser engraver the pattern is printed on GO twice in the same direction to achieve good results, i.e., better coverage and high conductivity.

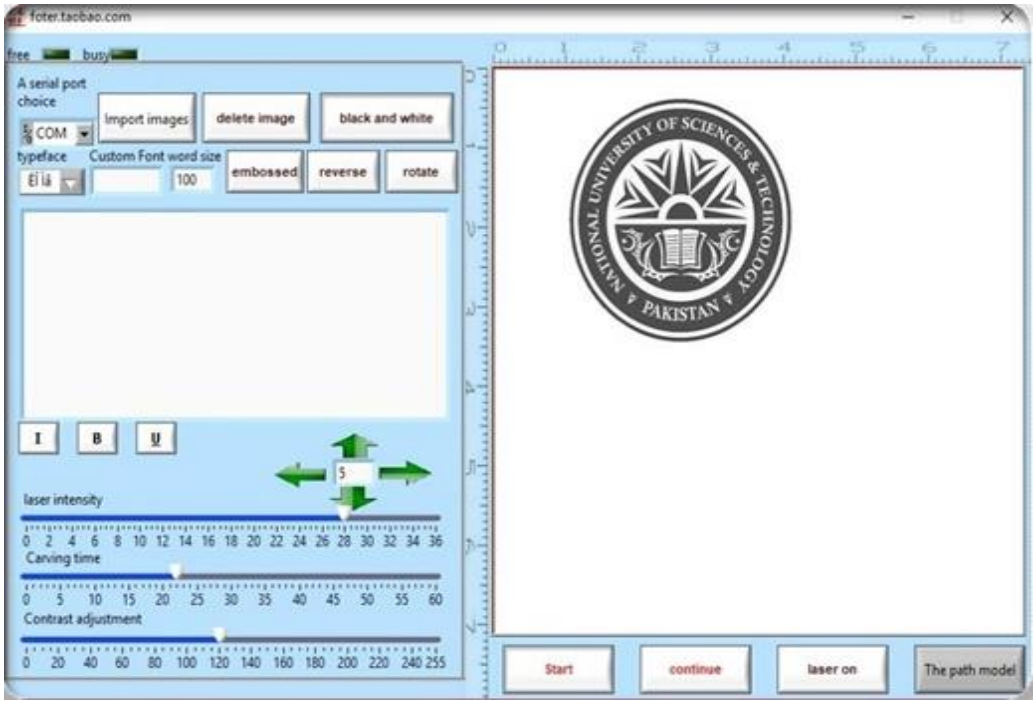

Fig 16: Laser Software screenshot used to instruct the laser engraver by using laptop

After laser scribing this device is further sent for material characterization by using SEM, RAMAN and XRD which is further described in chapter 4.

3.2.3 CONNECTIONS:

The last step is to apply connections to this conductive scribed area for output measurement. Copper tape is attached to the poles of the conductive pattern by using silver paste until dried and attached with the conductive area of the device for creating the output pathway. In the end we drop cast the PDMS mixture into the already prepared device to seal the connections and to avoid buckling. The same method of drying PDMS layer is used that is mention earlier.

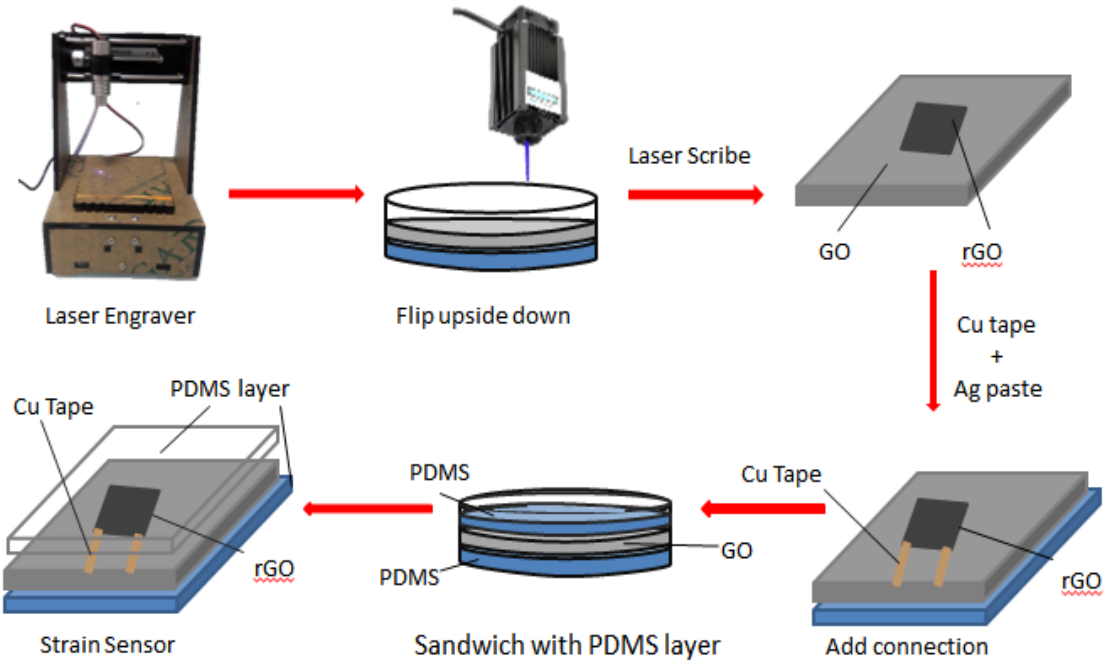

Fig 17: Laser scribing process of GO to convert it into RGO and implantation of connections for strain measurement.

After successfully fabricating, the excess material was removed and the device turned out to be in the square shape. The visual image of the final fabricated device is shown in fig 18.

Fig 18: The visual image of RGO PDMS strain sensor

3.3 ELECTRONIC SKIN PRESSURE SENSOR:

An electronic skin of strain sensors in a 2 × 2 array configuration has been prepared by using the same laser scribing method. The image has been prepared by using Adobe Illustrator with the precision of pixels that can be seen in the Fig 19. Blue blocks are the strain sensors that measure strain while the black lines are the connections. On the left of the image, the first input connection is attached to every strain sensor while the output can be calculated by the output sources of each sensor. The force is applied to the device as per unit area of strain sensor depicted as pressure therefore causes change in resistance. The pressure can be calculated by the formula:

P = F/A_____ (iii)

The sensitivity of pressure sensor can be calculated in per Pascal by using the formula.

$$= \frac{\Delta R}{R} / \frac{\Delta P}{P}$$

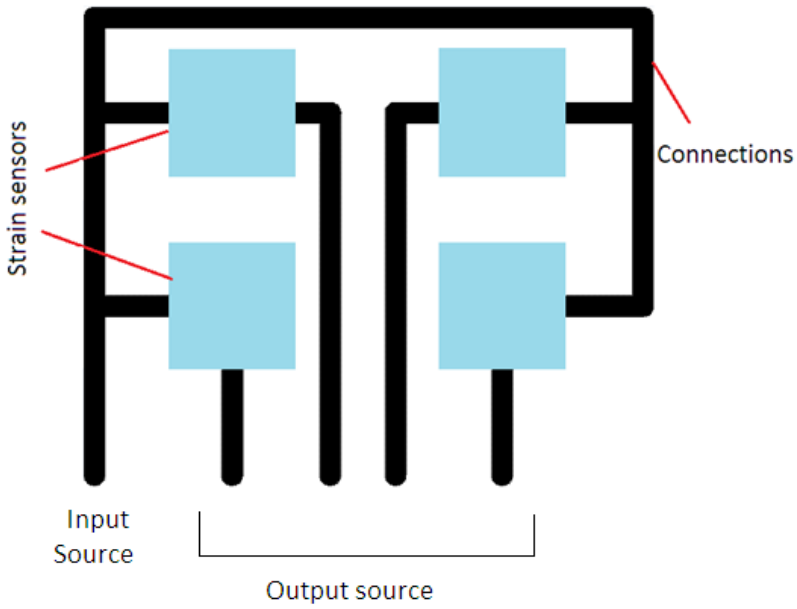

Fig 19: Electronic skin developed using 2 × 2 strain sensor array with connections strategy

The image of the laser engraved device is shown in fig 20 by using the same method used for fabrication of strain sensor.

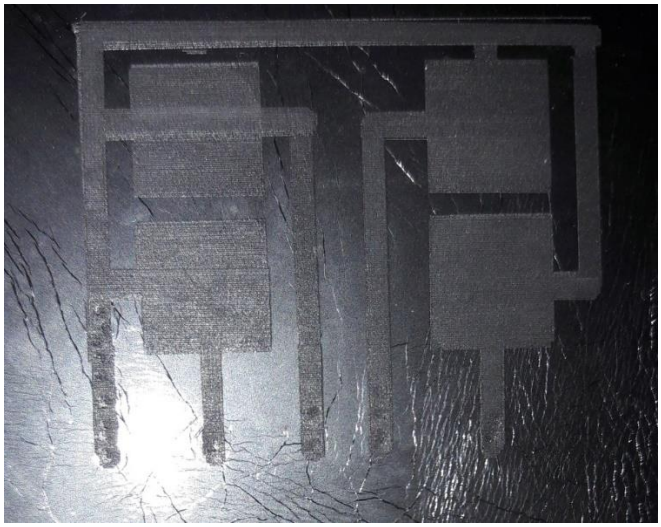

Fig 20: Laser scribed pressure sensor device used for electronic skin

3.4 HAND TEST FOR MUSCLE MOVEMENT DETECTION:

Sample is firstly clean and then attached to the joint of the hand by using double sided tape. A visible measurement has been taken by moving the joint. Change in resistance shows the change is strain. Calculation of resistance was done by using a digital multi-meter. This strain was successfully attached to the hand for 20 hours with normal washing and daily chores. Here are some of the pictures attached.

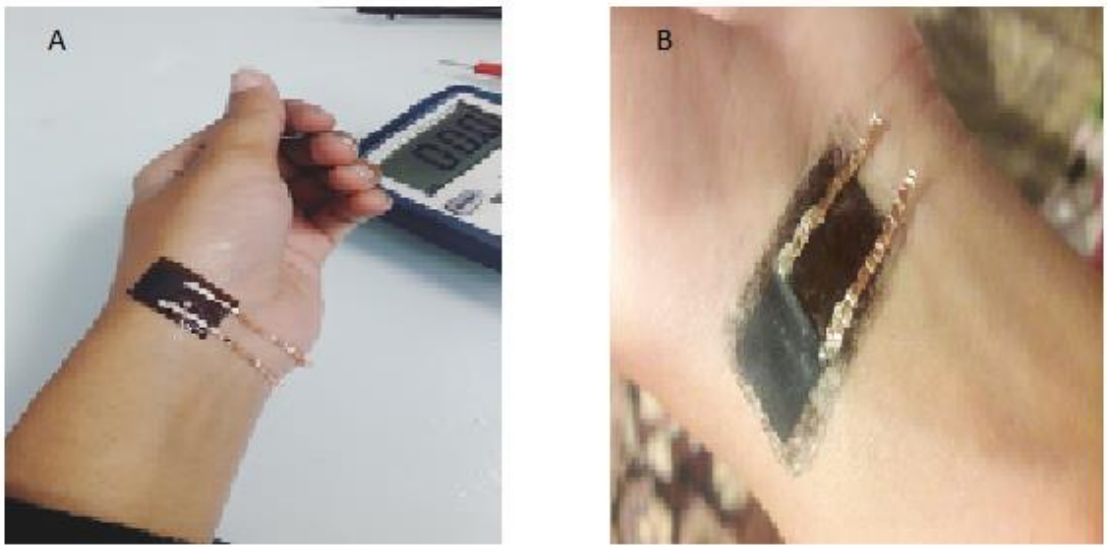

Fig 21: (A) Shows the sensor attached to the hand. (B) The image after 20 hours of attachment when the sensor was removed.

3.5 SIX AXIS TEST RIG:

This homemade test rig was assembled to measure the strain sensor characteristics across six degrees of freedom (6 DOF). The special feature of this rig lies in its ability to actuate 6x different strain conditions i.e., stretching (2 DOF), bending (2 DOF) and torsion (2 DOF). Previously strain was measured through a local firm by sending the device to the concerning person. Failure to coordinate or misalignment in the result caused delay. Therefore, a project was taken up to make the test rig within our lab. The first and second version of the test rig was manufactured using mechanical and electric actuation, while a third version is under development which uses electronic actuation.

Currently, an electrically actuated strain test rig (second version) is being used and an image of the second version is displayed in Fig: 23 to visually show how it works. In Fig: 22, the test rig contains two clamps to hold the sample in place as this figure shows the red clamp is fixed and the green one can move in opposite directions (stretching), can rotate (torsion). A nob is used to loose and tighten up the clamps after placing the sample. For the bending purpose a new silver color clip has been introduced in this rig which can be moved in a 3D direction.

Fig 22: Clamps to hold the device that can move up, down and, twist on either side.

After placing the sample in between, the clamps, readings can be taken from the connections of the fabricated device. Another advancement that has been introduced is the connection with the fabricated device as we need continuous readings so the wood base stand has been established which has crocodile clips to attach to the fabrication device from one side and the other side is connected with the multi-meter. This wooden stand prevents connection breakage Fig: 23.

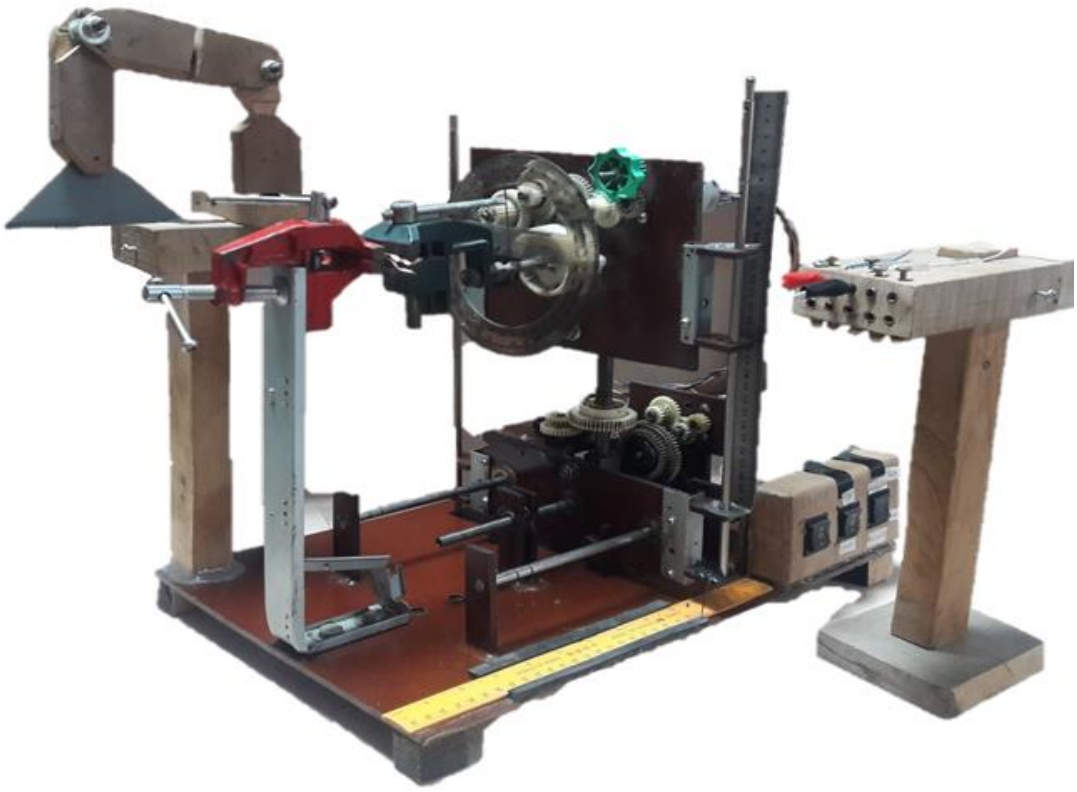

Fig 23: Test Rig used to apply strain on the device to measure its sensitivity.

This Test Rig provides three kinds of tests. Some of the explanation are provided below to explain the working of the test rig.

Tensile test:

Moving the green clamp on the opposite side of red one along the X direction according to the scale measurement can stretch a sample. Strain measurements can be taken by stretching. The compression measurements can be taken by moving the green clamp towards the red clamp but the sample buckles instead

Bending:

To apply bending strain onto the strain sensor, both clamps hold a sensor precisely at the same level from ground. A wooden base clip is adjusted in between both clamps upside the sensor and then the green clamps move along Y axis in upward direction to create a bending effect.

Torsion test:

To apply torsion, strain the clamp can move along the angle either in the clockwise or anti-clockwise direction. Red clamp is used as the referral angle to the angle where green clamp is pointed.

CHAPTER 4: RESULTS AND DISCUSSION

4.1 MATERIAL CHARACTERIZATION

To identify the structural and chemical changes and their unique behavior some material characterization was performed to acknowledge the presence of required material using XRD, SEM, and RAMAN. XRD and RAMAN were executed to identify and confirm the conversion of GO into RGO. To inspect the surface of material SEM was performed.

4.1.1 RAMAN SPECTROSCOPY:

Raman spectroscopy (BWS415-532S, USA) was performed to understand the defect structure, doping level and molecular vibrations of the material. The samples of GO were prepared and dried on a glass slide and then laser scribed to make RGO. The glass slide is used to avoid background noise during peak analysis. The D and G peaks tell us about the material property. The D peak depicts the defect structure of carbon lattice structure mainly presence of the oxygen containing functional groups in the sp^3 hybridized structure [125]. While the shift in G peak represents the addition of material as doping or subtraction of material as reduction. Right shift indicates the doping level and the left shift specifies the reduction process. Intensity of D peak of GO is slightly lower than RGO which demonstrates that C-C bond has been recovered [126].

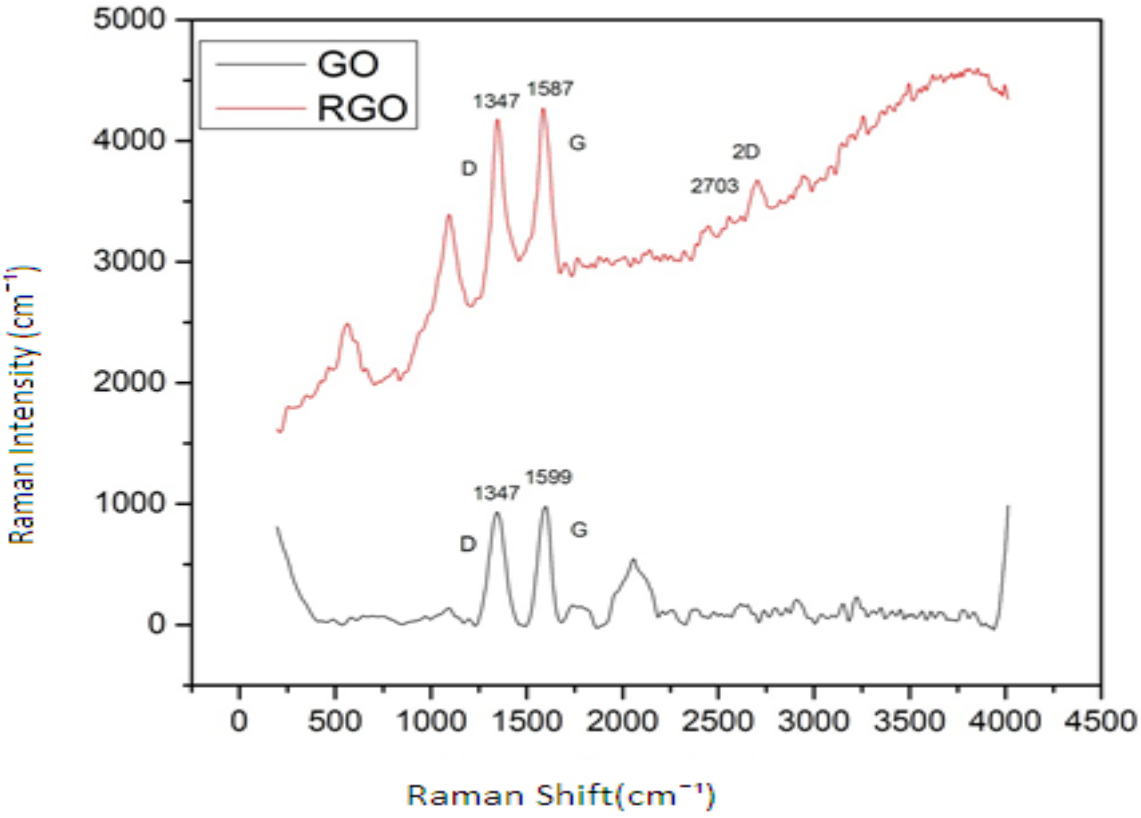

Fig 24: Raman spectroscopy graph for GO and RGO

RAMAN spectroscopy of GO shows D peak at 1350cm^{-1} and G peak at 1580cm^{-1}. While 2D of RGO shows around 2700cm^{-1} [123]. The left shift in G peak of RGO from 1599 to 1587 authenticates the reduction has taken place. The 2D peak in RGO arises in the absence of defects (functional groups) [127] and represents the multi-layer structure. This 2nd order reflection also depicts the presence of multilayer structure. The ratio of I^{2d}/I^{g} tells us the numbers of layers whether its bilayer, multilayer or single. If $I^{d}/I^{g} > 1$ the material have monolayer structure and if I^{d}/I^{g} is around 1, this represents bilayer structure while $I^{d}/I^{g} < 1$ represents the multi-layer morphology [126].

For GO

$$\frac{I^{d}}{I^{g}} = 0.97$$

For RGO

$\frac{I^d}{I^g} = 0.95$

$\frac{I^{2d}}{I^g} = 0.36$

I^d/I^g of RGO is less than GO, which indicates the partial healing of π bond conjugated hexagonal structure of C-C bond after laser reduction [125].

4.1.2 X-RAY DIFFRACTION:

XRD was performed on STOE θ-θ XRD Diffractometer. Sample was prepared the same way the device has been prepared. XRD is used to detect the components in that specific material. The Cu source having wavelength 1.54Å of STOE θ-θ XRD Diffractometer is used in this specific type of XRD.

The diffraction graph of XRD shows diffraction peak of GO at 2Θ (10.75˚) by (001) plane, which is due to oxygen containing functional groups. Sharp peak tells us about the ordered structure of the material. When converted from GO to RGO this peak reduce its intensity which depicts the removal of functional group and another broad peak is observed at 22.1˚ in plane (002) [128] broadening proclaims that the material is in disorder structure and it also depicts the presence of multilayer domain [129].

D spacing is actually the distance between adjacent GO sheets. GO have higher d spacing than RGO due to the presence of functional groups [128]. This can be calculated by the Bragg's law.

$\lambda = 2d \sin\theta$_____(iv)

To find the d spacing, the equation is rearranged.

$d = \frac{\lambda}{2 \sin\theta}$

The wavelength here is the one from the x-ray source. The wavelength of x-ray is 1.54Å. While θ is an angle taken from peak position like 2θ.

Table VII: D-spacing difference of GO and RGO.

	Θ	**d spacing**
GO	5.375	8.22Å
RGO	11.05	4.02Å

Here we can see the difference in d-spacing caused by functional groups.

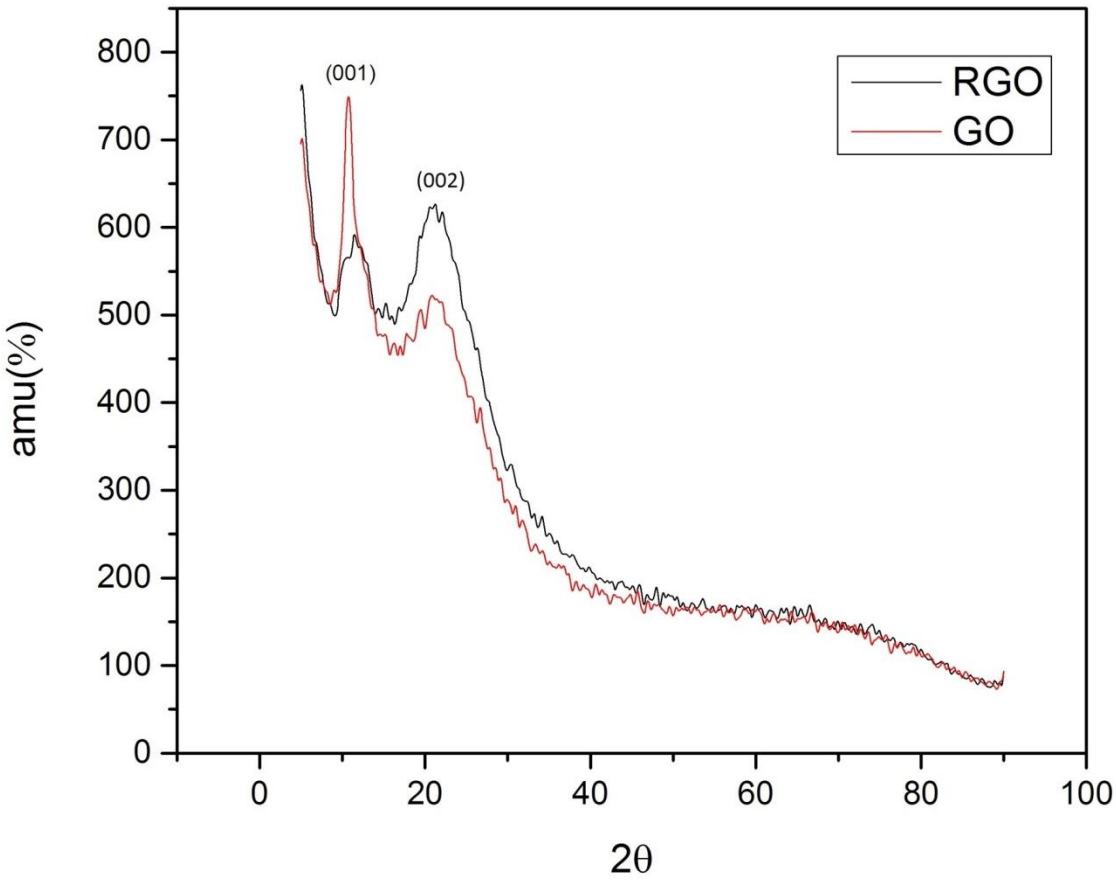

Fig 25: X-ray diffraction spectroscopy graph for GO and RGO

4.1.3 SCANNING ELECTRON MICROSCOPY:

SEM was performed using JEOL analytical SEM (JEOL-JSM-6490LA). Sample of GO was prepared on a PDMS substrate and then laser scribed. The sample was coated with gold and subjected to SEM. It was performed to study the surface morphology of graphene oxide and reduced graphene oxide. As exhibited in Fig: 26, panel (a) shows the surface of GO which is very smooth and laser scribed RGO is depicted by the rough surface on the left side of the image. The smoothness of GO shows single layer surface while multi-layer structure has been shown by rough RGO structure. Panel (b) shows the patterned surface of laser scribed RGO which clearly shows the porous structure. Panel (c) depicts the magnified surface of RGO.

Laser causes oxygen-containing functional groups to be removed in the form of gasses. That gasses intercalate between the layers of graphene oxide leaving behind the swelled surface of RGO (f) [126]. These gases create air gaps in between each layer of RGO while GO have more densely packed layers than RGO. These loosely packed sheets then aid in sensing strain. Panel (d) shows the layer thickness of GO which is very thin while panel (e) shows the layer thickness of RGO which is clearly thicker than GO.

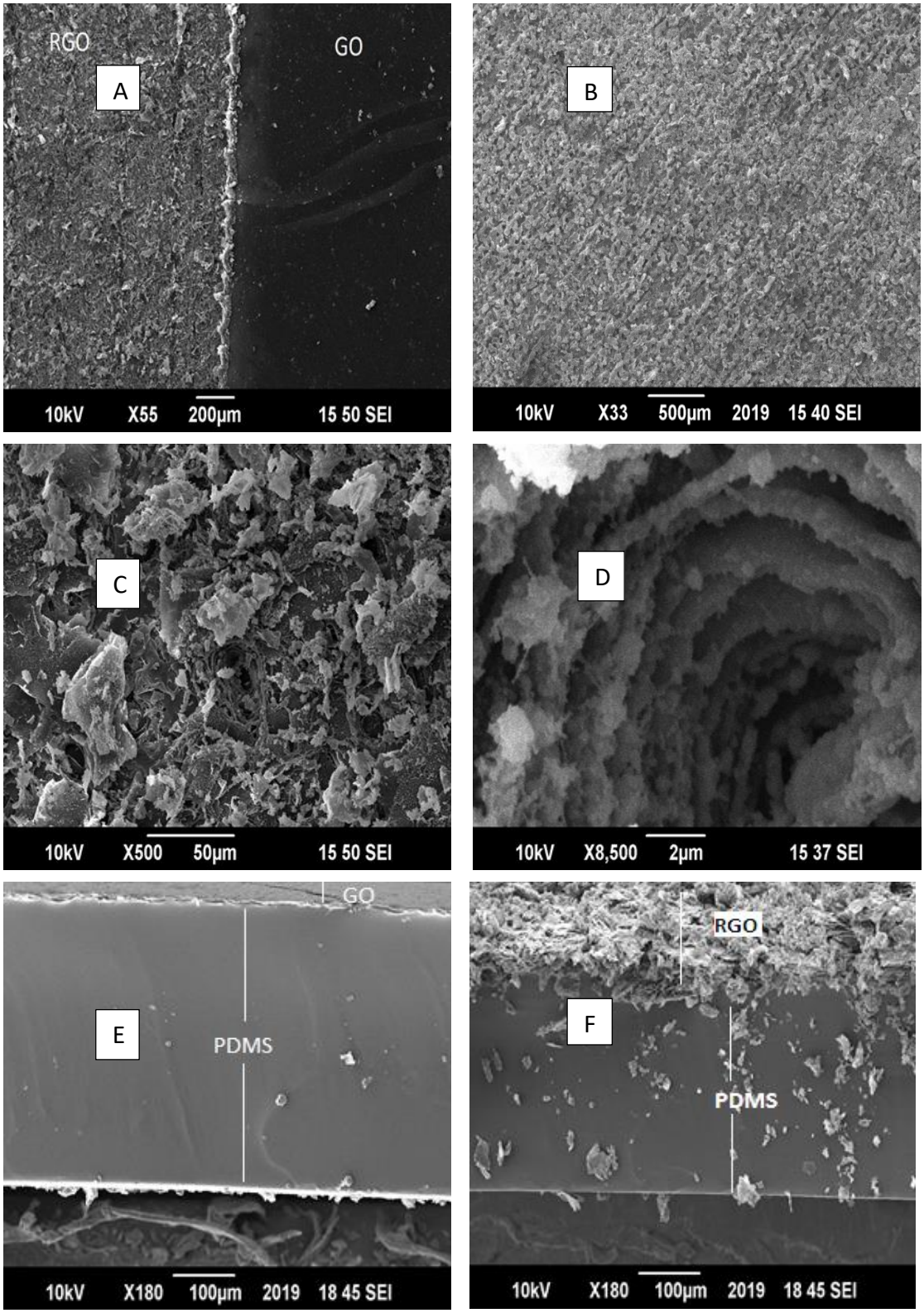

Fig 26: Scanning electron microscopy of GO and RGO at different magnifications. A) difference between GO and RGO, B) pattern structure of RGO, C) roughness of RGO layer after reduction, D) flacks of layers, E, F) thickness of GO and thickness of RGO

4.2 **LASER CHARACTERIZATION:**

Laser characterization was performed at National center of Physics, Islamabad. Some of the tests were performed to find laser wavelength and power range. This laser has a wavelength of 440 to 445 nm as shown in panel (c) with the pointer width of the laser is 1.5 nm when focused. The power range to be found out for this laser is from 50 to 500mW with respect to the software division shown in panel (d). This work has been done at a 50 to 100mW power range.

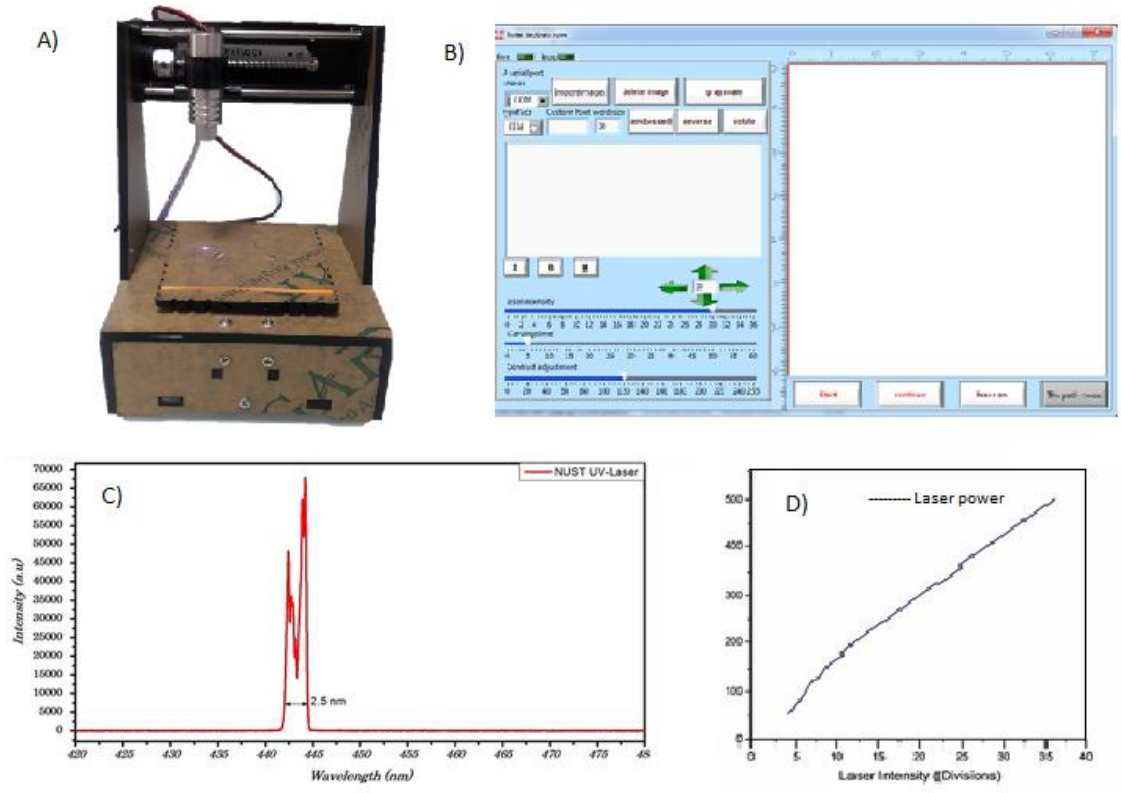

Fig 27: (A) laser engraver and (B) screenshot of laser software (C) wavelength of laser plot (D) Power vs division on the software plot

4.2.1 MECHANISM OF CONVERSION OF GO INTO RGO:

Laser is used to draw a pattern onto GO at ambient temperature and pressure. Laser converts GO into RGO that means from non-conductive to conductive pattern. Conversion has been done on the principle of photothermal/photochemical reduction [130]. There are number of papers that describe the mechanism of laser conversion. It's been found that the process of surface reduction takes place depending upon the

wavelength of the laser [131, 132]. The wavelength of laser higher than 390nm causes the photo-thermal reduction.

Laser provides the very high temperature range in between ~2500-3000°C and this high temperature removes the oxygen containing functional groups and converts them into gases that invades in between graphene oxide layers cause the swelling of the reduced area and create spaces between each layer [65].This conductive pattern is then used to sense strain/pressure.

4.3 DEVICE CHARACTERIZATION:

These strain sensors were made to sense different types of strain when applied. These strains were applied by using a locally manufactured test-rig as shown in section 3.5 Samples were prepared and adjusted between the clips of the device to apply strain. An electrical nob is used to apply strain on the device. The output was calculated by using a digital multi-meter. There are three different types of strain measurement that have been done on this device.

- Stretching (1 DOF)
- Bending (2 DOF)
- Torsion (2 DOF)

4.3.1 STRETCHING:

Stretching test was performed by using a test-rig. Resistance change was calculated by using a digital multi-meter with respect to change in length. These graphs show the ratio between changes in resistance upon applying strain percent after stretching the device. Resistance change in the device works on the mechanism of overlapping area of reduced graphene oxide flaky sheets upon stretching. The overlapping areas of sheets decreases, thus persuading the resistance to increase. Stretching the device shows linear change at start from 0 to 140% strain. After further stretching to 240% strain this sensor shows the sudden increase in the resistance is due to cracks production in the reduced graphene oxide layer. Upon maximum strain these cracks widen and breakout conductivity paths cause the drastic increase in resistance. This shows us that this sensor works perfectly till 140% strain.

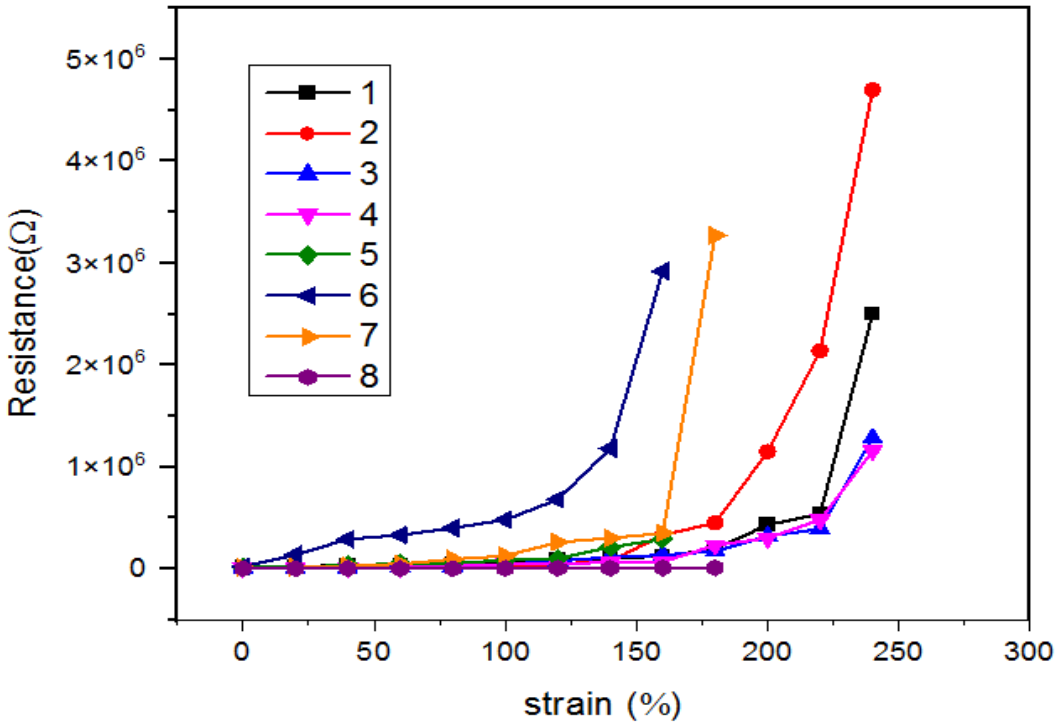

Fig 28: Individual behavior of each strain sensor device for "stretching".

Fig 28 shows the individual behavior of each device prepared by the same fabrication method described in chapter 3. While fig 29 shows the average behavior of all the devices while linear behavior can be seen by red line in the graph. This linear behavior shows two separate regions. This also leads to the two different Gauge factors for stretching. The lower strain range of 0 to 140% has a GF of 12.12, while for higher strain range of 140% to 240%, the GF is 353.38.

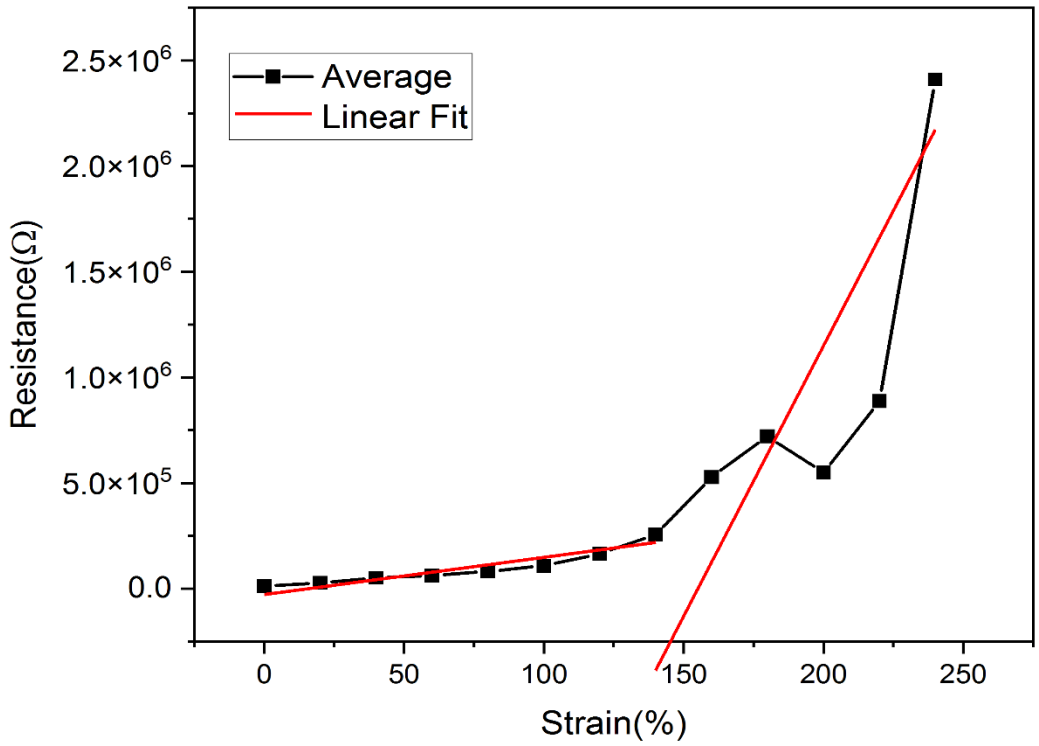

Fig 29: *Linear and average behavior of all the strain sensors after "stretching".*

4.3.2 BENDING:

The device has been set on test rig to apply bending. These results have been collected by changing length. Measurement has been done after each 2mm bending towards upward direction. This graph shows the data between resistance changes with respect to strain percent. The mechanism for the resistance change is the overlap area of sheets of reduced graphene oxide. Upon bending the device, the overlap area between the sheets reduces causing resistance to increase. This testing shows very similar behavior by each device with minute resistance change from each other. First graph (Fig: 30) shows the behavior of each device with respect to the other prepared by the same method described earlier. There are seven strain sensors that work best for bending. The starting point of each device has minute differences because of the cracks in the structure and also due to manual handling.

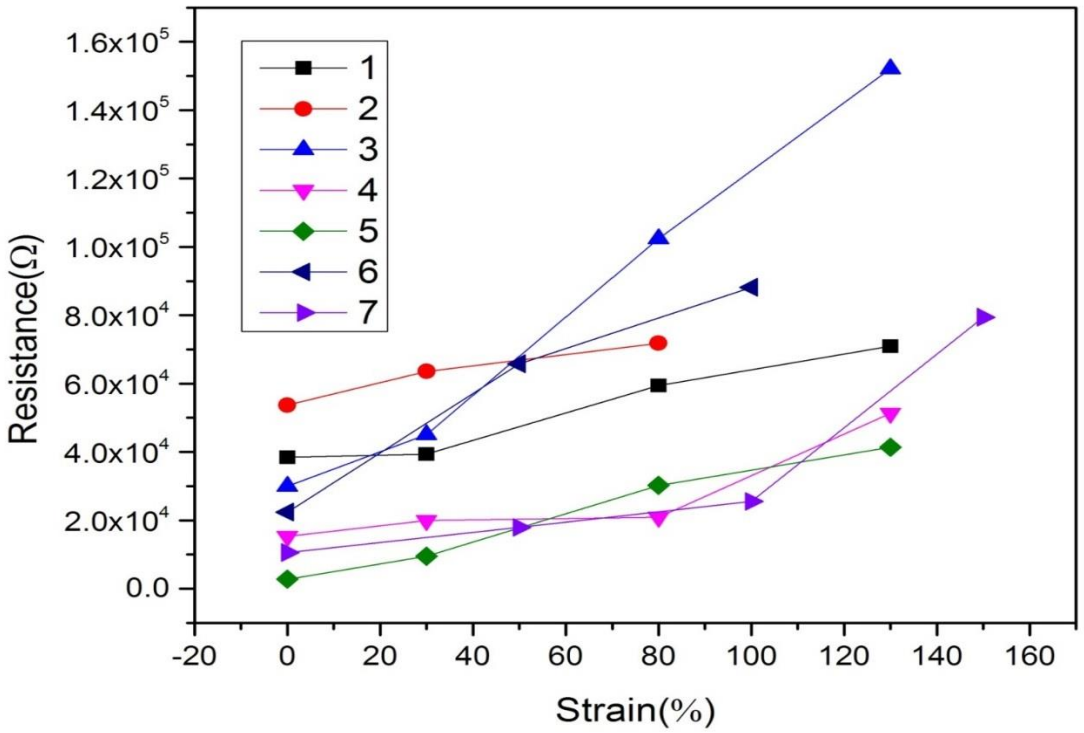

Fig 30: Individual behavior of each strain sensor device for "bending".

In the next graph Fig: 31 an average behavior of each device can be seen. Average and linear graph shows very indistinguishable results for strain percent. Device gave results for maximum 150% of strain which indicates that it has a very high bending range but the change in resistance is very linear resulting in a gauge factor GF of 3.468.

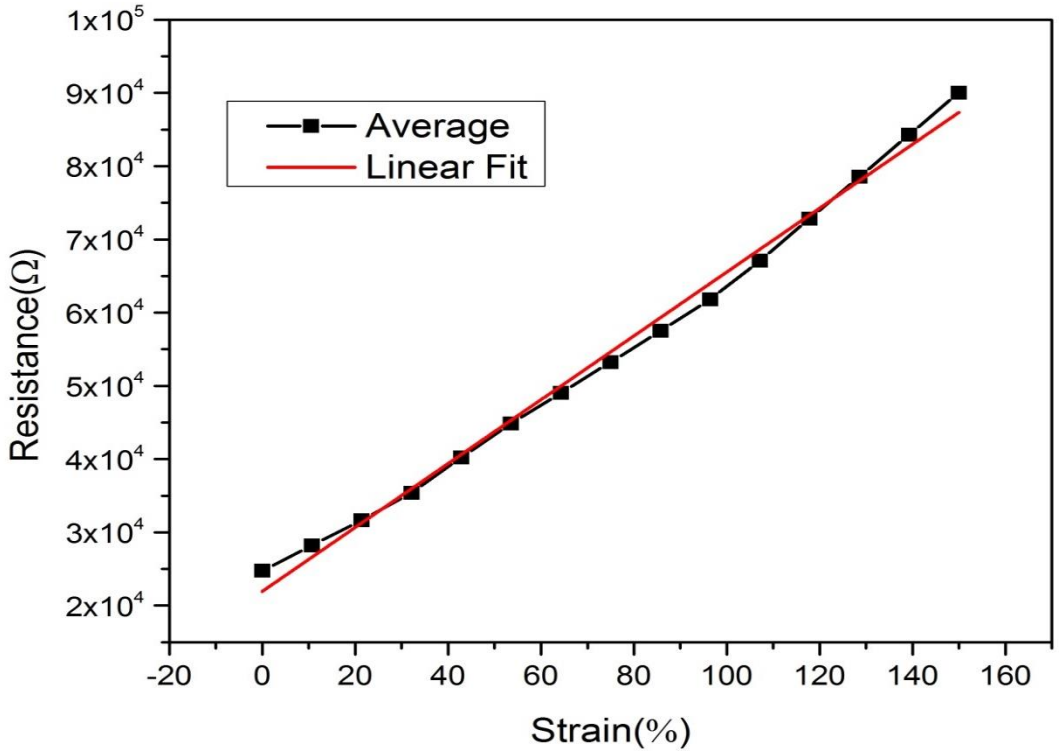

Fig 31: Linear and average behavior of all the strain sensors after "bending".

4.3.3 TORSION:

Test rig is used to apply the strain to twist the device in the form of angle. Each value has been measured after each 5 degrees. This graph shows the relation between resistance changes with respect to strain percent. This twisting mechanism changes the RGO flaky sheet's overlapping area which reduces the conductance and increases resistance. First graph in Fig: 32 shows the discrete behavior for each working device. The change is very linear from 0 to 11.12%. Then a sudden increase can be seen in the range from 11.12 to 16.68%. The cracks in RGO layer block the electron pathways, which cause a sudden increase in resistance.

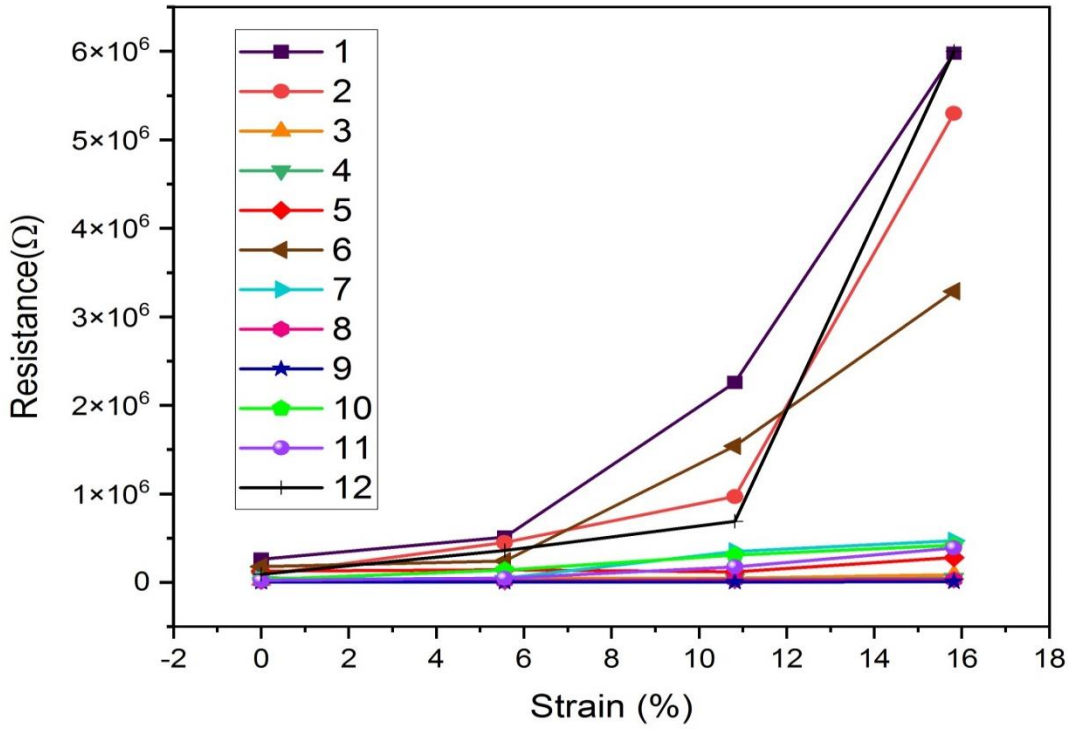

Fig 32: Individual behavior of each strain sensor device after "torsion".

The second graph shows the average behavior which shows a linear increase and then sudden increase in slope. This difference of behavior could be divided into two ranges, which gives a GF of 90.27 for the lower range but for the higher range, the GF increases to 227.13. The lower range has smaller deviations (smaller spread) between the devices because of the mechanism behind the sensitivity. This behavior leads us to the conclusion that strain sensor works best for the range of 0 to 11.12% strain.

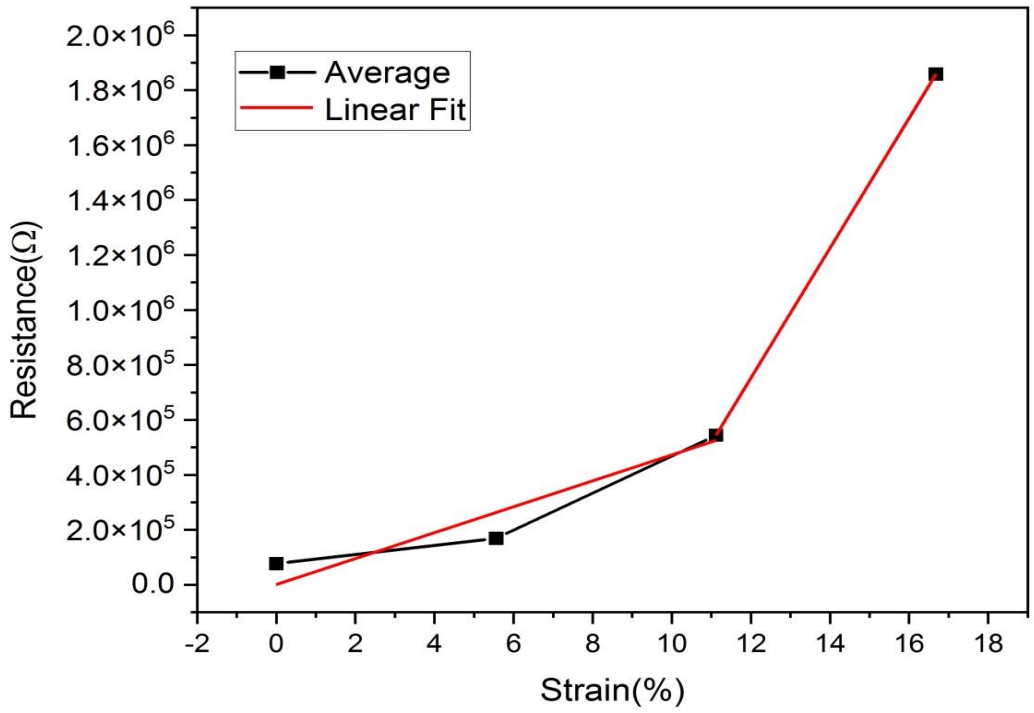

Fig 33: Average and linear behavior of all the strain sensors after "torsion".

4.4 SENSING MECHANISM OF PIEZORESISTIVITY IN RGO:

Structure of RGO sheets can be seen in the Fig: 34 whereby RGO consists of lots of sheets separated from each other unlike graphene. These sheets share their overlapping area with each other that provides pathways for current. When the sample is stretched, the overlapping area of sheets reduces as shown in the stretched RGO producing more resistance in current pathways.

When the device is bent at some angle or length-wise, it also affects the overlapping area of RGO causing reduction in shared area. The more the shared area, the smaller the pathway for conducting electrons. The reduction in overlapping area results in high resistance. While the same can be said in the case of torsion while twisting the device at some angle [110].

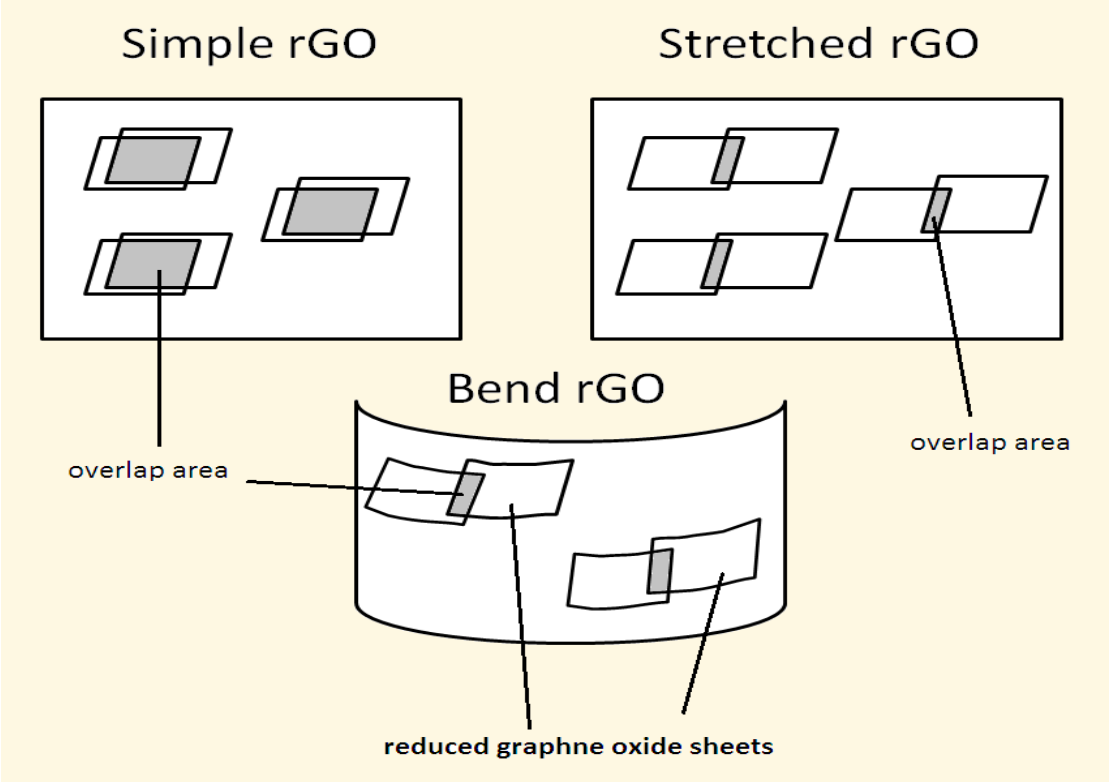

Fig 34: Mechanism of resistivity change in RGO for stretching and bending.

4.5 **MUSCLE MOVEMENT:**

Strain sensor was attached with the hand onto the wrist to measure the muscular motion of stretching and compression by moving the hand. Change in resistance has been observed. Time verses resistance graph of the regions of stretching and compression has been plotted. It can be seen in Fig: 35 that stretching causes the resistance to increase because the sensor was attached to hand, and upon stretching the overlap area of reduced graphene oxide sheets decrease causing resistance to increase. Likewise, in the case of compression, the resistance decrease due to the increased overlapping area (back to its stable state) of reduced graphene oxide sheets.

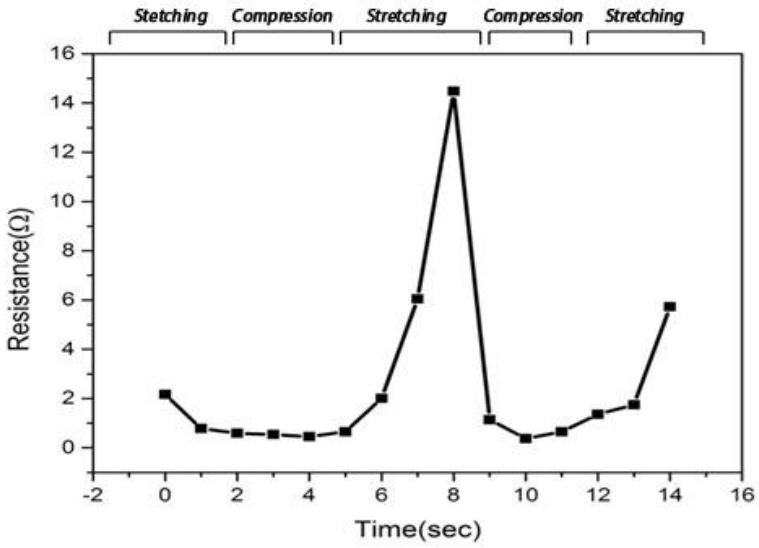

Fig 35: Time vs. resistance graph shows the resistance change upon stretching and compression.

4.6 COMPARISON FROM LITERATURE:

When comparing this research with the literature there are two main factors playing an important role in terms of sensor performance. The sensor needs to have good sensitivity within wide sensing range. As we can see in table (VIII) according to the literature one type of sensor have a very low sensing range with high gauge factor. And the other type has high sensing range but gauge factor drops to low. In comparison with the literature this work shows a very good sensitivity and sensing range for all strain types (torsion, stretching and bending).

Table VIII: Comparison between previous research and this work.

SENSING RANGE (strain %)	SENSTIVITY/GAUGE FACTOR(G.F)	*REF*
0.003%	54.2	[83]
0.098%	263.34	[78]
2%	233	[89]
5%	8.8	[81]
>7%	10^6	[82]
11.2%(Torsion)	90.27	*This work*
70%	2-14	[107]
140%(Stretching)	12.12	*This work*
150%(Bending)	3.468	*This work*
150%	0.05	[77]

CHAPTER 5: CONCLUSION AND FUTURE RECOMMENDATIONS

5.1 CONCLUSION:

- Reduced graphene oxide is used on PDMS to amalgamate their properties as a piezoresistive strain sensor.
- The single step fabrication by Laser is used to design then pattern on graphene oxide to alter their structure and convert it into reduced graphene oxide which shows conductive properties for sensing strain.
- Cracks were produced in RGO and GO that has been addressed by a specific preparation method and also sandwiching the device by PDMS.
- In this work, a new dimension is introduced in the category while it was not included in the previous research in our group. A fifth degree of freedom is introduced which contains stretching.
- An electric test rig was used whereas in the previous work in this group, a mechanical test rig was used.
- Strain sensor works for long range – it is working even after applying 160% strain to the device. That is beneficial in working for the devices which need long range strain measurement.
- The most reliable and highest gauge factor has been observed is 90.3 for torsion.
- The strain sensor in this work have simultaneously high sensitivity (GF) and can be measured over a large sensing range.

5.2 FUTURE RECOMMENDATIONS:

- Plasma etching on PDMS can be performed to increase the adhesion to layers.
- Researchers can work on pressure sensors with the same materials, with the intent to utilize the pressure sensors as electronic skin.
- Researchers can combine the properties of different material composites to work on the same pattern.
- Different applications e.g., artificial throat electronic skin, health monitoring of machines, ambient sensors, etc. can also be developed.

References

[1]. *Sensors: Technologies and Global Markets*. (2020): BCC Publishing.

[2]. *Resistance Strain Gauge Market Size, COVID-19 Impact Analysis By Regional Outlook(Europe, Asia Pacific, America[United States, Canada, Mexico, Brazil, Argentina, Columbia, Chile, Peru], Middle East And Africa), Industry Analysis Report, Growth Potential, Price Trend, Competitive Market Share, Market Statistics & Forecast 2021 - 2025*. (2021). p. 168.

[3]. *Global Strain Gauge Sensors Market- Industry Analysis and Forecast (2019-2027) – by Type, Mounting Type, End-User, and Region.* (2020): Maximize market research PVT. LTD.

[4]. Marques dos Santos, F.L. and B. Peeters, *On the use of strain sensor technologies for strain modal analysis: Case studies in aeronautical applications.* Review of Scientific Instruments, (2016). **87**(10): p. 102506.

[5]. Tao, L.-Q., et al., *An intelligent artificial throat with sound-sensing ability based on laser induced graphene.* Nature communications, (2017). **8**(1): p. 1-8.

[6]. Qiao, Y., et al., *Multilayer graphene epidermal electronic skin.* ACS nano, (2018). **12**(9): p. 8839-8846.

[7]. Ren, J., et al., *Environmentally-friendly conductive cotton fabric as flexible strain sensor based on hot press reduced graphene oxide.* Carbon, (2017). **111**: p. 622-630.

[8]. Jin, Y., et al., *Fabric-infused array of reduced graphene oxide sensors for mapping of skin temperatures.* Sensors and Actuators A: Physical, (2018). **280**: p. 92-98.

[9]. Souri, H. and D. Bhattacharyya, *Wearable strain sensors based on electrically conductive natural fiber yarns.* Materials & Design, (2018). **154**: p. 217-227.

[10]. Vetelino, J. and A. Reghu, *Introduction to sensors*. (2017): CRC press.

[11]. Tuteja, D., et al., *Detailed Survey on Motion Sensing.*

[12]. *Pressure Sensor Market Structure Analysis for the Period 2017 to 2023*. 10 june (2019); Available from: http://semiconductorreports.over-blog.com/2019/06/pressure-sensor-market-structure-analysis-for-the-period-2017-to-2023.html.

[13]. Kumar, S.S. and B. Pant, *Design principles and considerations for the 'ideal'silicon piezoresistive pressure sensor: a focused review.* Microsystem technologies, (2014). **20**(7): p. 1213-1247.

[14]. *Pressure Sensor Market worth $20.8 billion by 2025*.

[15]. *The History of Pressure Measurement*. Available from: https://www.sensorland.com/HowPage059.html.

[16]. *PRESSURE MEASUREMENT: Characteristics, Technologies and Trends*.

[17]. *Working Principle of a Pressure Sensor*. (2016), Variohm.

[18]. *Pressure sensors: The design engineer's guide*. Available from: https://www.avnet.com/wps/portal/abacus/solutions/technologies/sensors/pressure-sensors/.

[19]. *History of sensors*. Available from: https://www.sensorland.com/HistPage004.html.

[20]. DeHennis, A. and J. Chae, *Pressure sensors*, in *Comprehensive microsystems*. (2007), Elsevier. p. 101-133.

[21]. Stein, P.K., *A brief history of bonded resistance strain gages from conception to commercialization.* Experimental Techniques, (1990). **14**(5): p. 13-19.
[22]. *Structural analysis for personal helicopter airframe*. Available from: https://www.multipainkiller-studio.one/structural-analysis-for-personal-helicopter-airframe/.
[23]. Koushik, M., *Electronic Skin.* International Journal of Scientific & Engineering Research. **6**(5).
[24]. Kim, J., et al., *Stretchable silicon nanoribbon electronics for skin prosthesis.* Nature communications, (2014). **5**(1): p. 1-11.
[25]. Cheng, I.-C. and S. Wagner, *Overview of flexible electronics technology*, in *Flexible Electronics*. (2009), Springer. p. 1-28.
[26]. Akogwu, O.E., *Deformation and failure mechanisms in flexible and organic electronic structures*. (2010): Princeton University.
[27]. Okaniwa, H., et al. *Production and properties of a-Si: H solar cell on organic polymer film substrate*. in *16th Photovoltaic Specialists Conference*. (1982).
[28]. Okaniwa, H., et al., *Preparation and properties of a-Si: H solar cells on organic polymer film substrate.* Japanese Journal of Applied Physics, (1982). **21**(S2): p. 239.
[29]. Theiss, S. and S. Wagner, *Amorphous silicon thin-film transistors on steel foil substrates.* IEEE Electron Device Letters, (1996). **17**(12): p. 578-580.
[30]. Constant, A., et al. *Development of thin film transistor based circuits on flexible polyimide substrates*. in *Proc Electrochemical Society*. (1995).
[31]. *samsung*. (2020); Available from: https://www.samsung.com/pk/.
[32]. ; Available from: https://oled.com/.
[33]. Gleskova, H., et al., *Mechanical theory of the film-on-substrate-foil structure: Curvature and overlay alignment in amorphous silicon thin-film devices fabricated on free-standing foil substrates*, in *Flexible Electronics*. (2009), Springer. p. 29-51.
[34]. Nathan, A., et al., *Flexible electronics: the next ubiquitous platform.* Proceedings of the IEEE, (2012). **100**(Special Centennial Issue): p. 1486-1517.
[35]. MacDonald, W.A., *Engineered films for display technologies.* Journal of Materials Chemistry, (2004). **14**(1): p. 4-10.
[36]. Sheats, J.R. *Roll-to-roll manufacturing of thin film electronics*. in *Emerging Lithographic Technologies VI*. (2002). International Society for Optics and Photonics.
[37]. Fourkas, J., *Multiphoton lithography, processing and fabrication of photonic structures*, in *Laser Growth and Processing of Photonic Devices*. (2012), Elsevier. p. 139-161.
[38]. *Chapter 10 - MEMS Microrelay*, in *Space Microsystems and Micro/nano Satellites*, Z. You, Editor. (2018), Butterworth-Heinemann. p. 361-417.
[39]. Dyson, R.W., et al., *Specialty polymers*. (1987): Springer.
[40]. Mohammad, M.A., et al., *Fundamentals of electron beam exposure and development*, in *Nanofabrication*. (2012), Springer. p. 11-41.
[41]. Gan, Z., et al., *Three-dimensional deep sub-diffraction optical beam lithography with 9 nm feature size.* Nature communications, (2013). **4**(1): p. 1-7.
[42]. van Assenbergh, P., et al., *Nanostructure and microstructure fabrication: from desired properties to suitable processes.* Small, (2018). **14**(20): p. 1703401.

[43]. Gates, B.D., et al., *New approaches to nanofabrication: molding, printing, and other techniques.* Chemical reviews, (2005). **105**(4): p. 1171-1196.
[44]. Peng, L., et al., *Micro hot embossing of thermoplastic polymers: a review.* Journal of Micromechanics and Microengineering, (2013). **24**(1): p. 013001.
[45]. Semlyen, S.J.C.J.A., *Siloxane polymers*. 1993: Englewood Cliffs, N.J. : Prentice Hall, ©(1993). 673.
[46]. Heckele, M., W. Bacher, and K. Müller, *Hot embossing-the molding technique for plastic microstructures.* Microsystem technologies, (1998). **4**(3): p. 122-124.
[47]. Chou, S.Y., et al., *Sub-10 nm imprint lithography and applications.* Journal of Vacuum Science & Technology B: Microelectronics and Nanometer Structures Processing, Measurement, and Phenomena, (1997). **15**(6): p. 2897-2904.
[48]. Austin, M.D., et al., *Fabrication of 5 nm linewidth and 14 nm pitch features by nanoimprint lithography.* Applied Physics Letters, (2004). **84**(26): p. 5299-5301.
[49]. Ahn, S.H. and L.J. Guo, *High-speed roll-to-roll nanoimprint lithography on flexible plastic substrates.* Advanced materials, (2008). **20**(11): p. 2044-2049.
[50]. Hosseindokht, Z., et al., *Low cost flexible pressure sensor using laser scribed GO/RGO periodic structure for electronic skin applications.* Superlattices and Microstructures, (2020). **140**: p. 106470.
[51]. Ye, R., D.K. James, and J.M. Tour, *Laser-induced graphene.* Accounts of chemical research, (2018). **51**(7): p. 1609-1620.
[52]. Afentakis, T., et al., *Design and fabrication of high-performance polycrystalline silicon thin-film transistor circuits on flexible steel foils.* IEEE transactions on electron devices, (2006). **53**(4): p. 815-822.
[53]. Park, J., K. Shin, and C. Lee, *Roll-to-roll coating technology and its applications: A review.* International Journal of Precision Engineering and Manufacturing, (2016). **17**(4): p. 537-550.
[54]. Campo, E.A., *Selection of Polymeric Materials*. (2008), William Andrew. p. 350.
[55]. Bosq, N., et al., *Melt and glass crystallization of PDMS and PDMS silica nanocomposites.* Physical Chemistry Chemical Physics, (2014). **16**(17): p. 7830-7840.
[56]. Goosey, M., *Permeability of coatings and encapsulants for electronic and optoelectronic devices*, in *Polymer Permeability*. (1985), Springer. p. 309-339.
[57]. Jamieson, E. and A. Windle, *Structure and oxygen-barrier properties of metallized polymer film.* Journal of Materials Science, (1983). **18**(1): p. 64-80.
[58]. Vogt, B.D., et al., *X-ray and neutron reflectivity measurements of moisture transport through model multilayered barrier films for flexible displays.* Journal of applied physics, (2005). **97**(11): p. 114509.
[59]. Mata, A., A.J. Fleischman, and S. Roy, *Characterization of polydimethylsiloxane (PDMS) properties for biomedical micro/nanosystems.* Biomedical microdevices, (2005). **7**(4): p. 281-293.
[60]. Yogeswaran, N., et al., *New materials and advances in making electronic skin for interactive robots.* Advanced Robotics, (2015). **29**(21): p. 1359-1373.
[61]. Dahiya, R.S., et al., *Tactile sensing—from humans to humanoids.* IEEE transactions on robotics, (2009). **26**(1): p. 1-20.
[62]. Dahiya, R.S. and M. Valle, *Tactile sensing technologies*, in *Robotic tactile sensing*. (2013), Springer. p. 79-136.

[63]. Kaboli, M., A. Long, and G. Cheng, *Humanoids learn touch modalities identification via multi-modal robotic skin and robust tactile descriptors.* Advanced Robotics, (2015). **29**(21): p. 1411-1425.
[64]. Zhou, H., et al., *Robust and sensitive pressure/strain sensors from solution processable composite hydrogels enhanced by hollow-structured conducting polymers.* Chemical Engineering Journal, (2021). **403**: p. 126307.
[65]. Song, J., X. Wang, and C.-T. Chang, *Preparation and characterization of graphene oxide.* Journal of Nanomaterials, (2014). **2014**.
[66]. Zheng, Q., et al., *Graphene oxide-based transparent conductive films.* Progress in Materials Science, (2014). **64**: p. 200-247.
[67]. Schmiedova, V., et al., *Physical properties investigation of reduced graphene oxide thin films prepared by material inkjet printing.* Journal of Nanomaterials, (2017). **2017**.
[68]. Tencha, A., et al. *Synthesis of graphene oxide inks for printed electronics*. in *2017 IEEE International Young Scientists Forum on Applied Physics and Engineering (YSF)*. (2017). IEEE.
[69]. Mohan, V.B., et al., *Characterisation of reduced graphene oxide: Effects of reduction variables on electrical conductivity.* Materials Science and Engineering: B, (2015). **193**: p. 49-60.
[70]. Qureshi, T.S. and D.K. Panesar. *A comparison of graphene oxide, reduced graphene oxide and pure graphene: early age properties of cement composites*. in *2nd RILEM Spring Convention & International Conference on Sustainable Materials, Systems and Structures. Rovinj, Croatia*. (2019).
[71]. Graphenea. *Reduced Graphene Oxide: Properties, Applications and Production Methods*. 01 February (2021); Available from: https://www.azonano.com/article.aspx?ArticleID=4041.
[72]. Liu, L., et al., *Mechanical properties of graphene oxides.* Nanoscale, (2012). **4**(19): p. 5910-5916.
[73]. Teklu, A., et al., *Mechanical characterization of reduced graphene oxide using AFM.* Advances in Condensed Matter Physics, (2019). **2019**.
[74]. Bi, H., et al., *Ultrahigh humidity sensitivity of graphene oxide.* Scientific reports, (2013). **3**(1): p. 1-7.
[75]. Chang, W.-C., et al., *Quantifying surface area of nanosheet graphene oxide colloid using a gas-phase electrostatic approach.* Analytical chemistry, (2017). **89**(22): p. 12217-12222.
[76]. Kwon, K., Y. Jin Jo, and T.i. Kim, *Flexible Electronics.* Wiley Encyclopedia of Electrical and Electronics Engineering, (1999): p. 1-10.
[77]. Yamada, T., et al., *A stretchable carbon nanotube strain sensor for human-motion detection.* Nature nanotechnology, (2011). **6**(5): p. 296.
[78]. Liu, L., et al., *Bioinspired, Superhydrophobic, and Paper-Based Strain Sensors for Wearable and Underwater Applications.* ACS Applied Materials & Interfaces, (2020).
[79]. Park, J.W., et al., *Measurement of finger joint angle using stretchable carbon nanotube strain sensor.* PloS one, (2019). **14**(11): p. e0225164.
[80]. Wang, X., et al., *Highly sensitive and stretchable piezoresistive strain sensor based on conductive poly (styrene-butadiene-styrene)/few layer graphene composite fiber.* Composites Part A: Applied Science and Manufacturing, (2018). **105**: p. 291-299.

[81]. Mi, Q., et al., *RGO-coated elastic fibres as wearable strain sensors for full-scale detection of human motions.* Smart Materials and Structures, (2017). **27**(1): p. 015014.
[82]. Wang, Y., et al., *Wearable and highly sensitive graphene strain sensors for human motion monitoring.* Advanced Functional Materials, (2014). **24**(29): p. 4666-4670.
[83]. Naveed, S., et al. *A laser scribed graphene oxide and polyimide hybrid strain sensor*. in *Key Engineering Materials*. (2018). Trans Tech Publ.
[84]. Marra, F., et al., *Production and characterization of Graphene Nanoplatelet-based ink for smart textile strain sensors via screen printing technique.* Materials & Design, (2021). **198**: p. 109306.
[85]. Nakamura, A., et al., *A piezo-resistive graphene strain sensor with a hollow cylindrical geometry.* Materials Science and Engineering: B, (2017). **219**: p. 20-27.
[86]. Xu, S., et al., *Flexible, self-powered and multi-functional strain sensors comprising a hybrid of carbon nanocoils and conducting polymers.* Chemical Engineering Journal, (2021). **404**: p. 126064.
[87]. Gong, X., et al., *Piezoresistive strain sensors based on psyllium-carbon nanostructure skeletons.* Composites Part B: Engineering, (2021): p. 108610.
[88]. Qiu, A., et al., *Highly Sensitive and Flexible Capacitive Elastomeric Sensors for Compressive Strain Measurements.* Materials Today Communications, (2021): p. 102023.
[89]. Wang, B., et al., *Graphene/polydimethylsiloxane nanocomposite strain sensor.* Review of Scientific Instruments, (2013). **84**(10): p. 105005.
[90]. Xu, R., et al., *Facile fabrication of three-dimensional graphene foam/poly (dimethylsiloxane) composites and their potential application as strain sensor.* ACS applied materials & interfaces, (2014). **6**(16): p. 13455-13460.
[91]. Liao, X., et al., *Flexible and printable paper-based strain sensors for wearable and large-area green electronics.* Nanoscale, (2016). **8**(26): p. 13025-13032.
[92]. Long, Y., et al., *Molybdenum-carbide-graphene composites for paper-based strain and acoustic pressure sensors.* Carbon, (2020). **157**: p. 594-601.
[93]. Matsuzaki, R. and A. Todoroki, *Wireless flexible capacitive sensor based on ultra-flexible epoxy resin for strain measurement of automobile tires.* Sensors and Actuators A: Physical, (2007). **140**(1): p. 32-42.
[94]. Bhattacharjee, M., et al., *PEDOT: PSS Microchannel-Based Highly Sensitive Stretchable Strain Sensor.* Advanced Electronic Materials, (2020). **6**(8): p. 2000445.
[95]. Li, Y., et al., *Strain sensor with both a wide sensing range and high sensitivity based on braided graphene belts.* ACS applied materials & interfaces, (2020). **12**(15): p. 17691-17698.
[96]. Zhu, Y., et al., *Fabrication of low-cost and highly sensitive graphene-based pressure sensors by direct laser scribing polydimethylsiloxane.* ACS applied materials & interfaces, (2019). **11**(6): p. 6195-6200.
[97]. Chen, J., et al., *Polydimethylsiloxane (PDMS)-based flexible resistive strain sensors for wearable applications.* Applied Sciences, (2018). **8**(3): p. 345.
[98]. Lü, X., et al., *High sensitivity flexible electronic skin based on graphene film.* Sensors, (2019). **19**(4): p. 794.

[99]. Hanif, A., et al., *Stretchable, transparent, tough, ultrathin, and self-limiting skin-like substrate for stretchable electronics.* ACS applied materials & interfaces, (2018). **10**(32): p. 27297-27307.
[100]. Wang, S., et al., *Skin electronics from scalable fabrication of an intrinsically stretchable transistor array.* Nature, (2018). **555**(7694): p. 83-88.
[101]. Zhan, Z., et al., *Paper/carbon nanotube-based wearable pressure sensor for physiological signal acquisition and soft robotic skin.* ACS applied materials & interfaces, (2017). **9**(43): p. 37921-37928.
[102]. Razavi, M. and A.S. Thakor, *An oxygen plasma treated poly (dimethylsiloxane) bioscaffold coated with polydopamine for stem cell therapy.* Journal of Materials Science: Materials in Medicine, (2018). **29**(5): p. 1-14.
[103]. Wang, S., L. Lin, and Z.L. Wang, *Triboelectric nanogenerators as self-powered active sensors.* Nano Energy, (2015). **11**: p. 436-462.
[104]. Qi, X., et al., *Mulberry paper-based graphene strain sensor for wearable electronics with high mechanical strength.* Sensors and Actuators A: Physical, (2020). **301**: p. 111697.
[105]. Jia, Z., et al., *Constructing conductive titanium carbide nanosheet (MXene) network on polyurethane/polyacrylonitrile fibre framework for flexible strain sensor.* Journal of Colloid and Interface Science, (2021). **584**: p. 1-10.
[106]. Boland, C.S., et al., *Sensitive, high-strain, high-rate bodily motion sensors based on graphene–rubber composites.* ACS nano, (2014). **8**(9): p. 8819-8830.
[107]. Amjadi, M., et al., *Highly stretchable and sensitive strain sensor based on silver nanowire–elastomer nanocomposite.* ACS nano, (2014). **8**(5): p. 5154-5163.
[108]. Tolvanen, J., J. Hannu, and H. Jantunen, *Stretchable and washable strain sensor based on cracking structure for human motion monitoring.* Scientific reports, (2018). **8**(1): p. 1-10.
[109]. Lee, D.-J. and D.Y. Kim, *based, hand-painted strain sensor based on ITO nanoparticle channels for human motion monitoring.* IEEE Access, (2019). **7**: p. 77200-77207.
[110]. Park, J., et al., *Tactile-direction-sensitive and stretchable electronic skins based on human-skin-inspired interlocked microstructures.* ACS nano, (2014). **8**(12): p. 12020-12029.
[111]. Arshak, K., D. McDonagh, and M. Durcan, *Development of new capacitive strain sensors based on thick film polymer and cermet technologies.* Sensors and Actuators A: Physical, (2000). **79**(2): p. 102-114.
[112]. Lin, J.-T., et al., *Development of capacitive pure bending strain sensor for wireless spinal fusion monitoring.* Sensors and Actuators A: Physical, (2007). **138**(2): p. 276-287.
[113]. Xu, M., et al., *Novel and dual-mode strain-detecting performance based on a layered NiO/ZnO p–n junction for flexible electronics.* Journal of Materials Chemistry C, (2020). **8**(4): p. 1466-1474.
[114]. Wu, J.M., et al., *Ultrahigh sensitive piezotronic strain sensors based on a ZnSnO3 nanowire/microwire.* ACS nano, (2012). **6**(5): p. 4369-4374.
[115]. You, R., et al., *Laser fabrication of graphene-based flexible electronics.* Advanced Materials, (2020). **32**(15): p. 1901981.
[116]. Huang, K., et al., *Ultrasensitive MWCNT/PDMS composite strain sensor fabricated by laser ablation process.* Composites Science and Technology, (2020). **192**: p. 108105.

[117]. Chhetry, A., et al., *Black Phosphorus@ Laser-Engraved Graphene Heterostructure-Based Temperature–Strain Hybridized Sensor for Electronic-Skin Applications.* Advanced Functional Materials, (2020): p. 2007661.
[118]. Kong, X., et al., *Laser-Scribed N-Doped Graphene for Integrated Flexible Enzymatic Biofuel Cells.* ACS Sustainable Chemistry & Engineering, (2020). **8**(33): p. 12437-12442.
[119]. Cho, E.-C., et al., *PEDOT-modified laser-scribed graphene films as bginder–and metallic current collector–free electrodes for large-sized supercapacitors.* Applied Surface Science, (2020). **518**: p. 146193.
[120]. Park, C., et al., *Fabrication of electrochromic devices by laser patterning of spin-sprayed transparent conductive Ga: ZnO films.* Ceramics International, (2020).
[121]. Li, J., et al., *Effects of Laser-Scribed Mo Groove Shape on Highly Efficient Zn (O, S)-Based Cu (In, Ga) Se2 Solar Modules.* Solar RRL, (2020). **4**(4): p. 1900510.
[122]. Nasir, F. and M.A. Mohammad, *Investigation of Device Dimensions on Electric Double Layer Microsupercapacitor Performance and Operating Mechanism.* IEEE Access, (2020). **8**: p. 28367-28374.
[123]. Wolf, M.P., G.B. Salieb-Beugelaar, and P. Hunziker, *PDMS with designer functionalities—Properties, modifications strategies, and applications.* Progress in Polymer Science, (2018). **83**: p. 97-134.
[124]. Suleman, M.S., K. Lau, and Y. Yeong, *Characterization and performance evaluation of PDMS/PSF membrane for CO2/CH4 separation under the effect of swelling.* Procedia engineering, (2016). **148**: p. 176-183.
[125]. Park, R., et al., *One-step laser patterned highly uniform reduced graphene oxide thin films for circuit-enabled tattoo and flexible humidity sensor application.* Sensors, (2018). **18**(6): p. 1857.
[126]. Tian, H., et al., *Laser-scribing technology for wafer-scale graphene devices.* Advances in Carbon Nanostructures, (2016): p. 63.
[127]. Gayathri, S., et al., *Synthesis of few layer graphene by direct exfoliation of graphite and a Raman spectroscopic study.* Aip Advances, (2014). **4**(2): p. 027116.
[128]. Rajaura, R.S., et al., *Role of interlayer spacing and functional group on the hydrogen storage properties of graphene oxide and reduced graphene oxide.* International Journal of Hydrogen Energy, (2016). **41**(22): p. 9454-9461.
[129]. Saini, P., R. Sharma, and N. Chadha, *Determination of defect density, crystallite size and number of graphene layers in graphene analogues using X-ray diffraction and Raman spectroscopy.* Indian Journal of Pure & Applied Physics (IJPAP), (2017). **55**(9): p. 625-629.
[130]. Arul, R., et al., *The mechanism of direct laser writing of graphene features into graphene oxide films involves photoreduction and thermally assisted structural rearrangement.* Carbon, (2016). **99**: p. 423-431.
[131]. Lin, J., et al., *Laser-induced porous graphene films from commercial polymers.* Nature communications, (2014). **5**(1): p. 1-8.
[132]. Zhang, H. and Y. Miyamoto, *Graphene production by laser shot on graphene oxide: An ab initio prediction.* Physical Review B, (2012). **85**(3): p. 033402.